1964-12-11

An Improved Method of Neutron Spectroscopy Using Threshold Detectors

Kohler, Arthur Degen Jr.

California. Univ., Berkeley. Lawrence Radiation Lab

UCRL-11760

UNIVERSITY OF CALIFORNIA
Lawrence Radiation Laboratory
Berkeley, California

AEC Contract No. W-7405-eng-48

AN IMPROVED METHOD OF NEUTRON SPECTROSCOPY USING THRESHOLD DETECTORS

Arthur Degen Kohler, Jr.

(Master's Thesis)

December 11, 1964

AN IMPROVED METHOD OF NEUTRON SPECTROSCOPY USING THRESHOLD DETECTORS

Contents

AN IMPROVED METHOD OF NEUTRON SPECTROSCOPY USING THRESHOLD DETECTORS

Arthur Degen Kohler, Jr.*

Lawrence Radiation Laboratory
University of California
Berkeley, California

December 11, 1964

ABSTRACT

An improved technique of measuring neutron-energy spectra in the range 2.5 to 30 MeV has been developed. In this technique threshold detectors are exposed to the unknown neutron flux. The activities of residual nuclei from (n, p), (n, α), and (n, 2n) threshold reactions are measured by gamma-spectrum analysis. Experimental excitation functions are used. Measured activities and cross sections form a set of integral equations which are solved for the neutron spectrum by using a least-squares technique.

Neutron-reaction cross sections are not well known above about 20 MeV, and 30 MeV is selected as the highest energy for which this method is feasible based on available data. An approximate correction is made to measured activities to account for activation caused by neutrons with energies above 30 MeV.

The previous technique, on which this work is based, was improved by:

(a) substitution of experimental reaction cross sections (from recently published literature) for those calculated from the continuum model of the nucleus;

---

*Lieutenant, Civil Engineer Corps, United States Navy.

(b) solution of the spectrum from the set of integral equations by a least-squares technique;

(c) calculation of the amount of activation of threshold detectors caused by neutrons with energies above 30 MeV within a thick concrete shield exposed to a 6.2-BeV proton beam.

Application of this improved technique is demonstrated in experiments with a $Be^{9}(d, n)B^{10}$ neutron source, and the neutron spectra in a thick concrete shield exposed to a 6.2-BeV proton beam.

I. INTRODUCTION

Activation of threshold detectors by (n, p), (n, α) and (n, 2n) reactions has been developed and demonstrated as a useful method of neutron spectroscopy in a previous study.[1] This method is applicable to the energy range of 2 to 30 MeV and is sufficiently sensitive to measure very small fluxes of the order of 1 to 100 n/cm^2 sec.

In this method, a number of different detectors, usually in the form of 4-in. diam metal discs are exposed to the unknown neutron flux. After exposure, the detectors are moved to a low-background counting facility. The gamma-ray spectrum of the activated detector is measured by using a NaI crystal, photomultiplier, and pulse-height analyser. Analysis of the gamma-ray spectrum identifies the radioactive nuclei and their decay rate. In application, a set of metal-disc detectors of aluminum, iron, cobalt, and nickel might be exposed to the neutron flux. In the aluminum disc one might observe gamma rays of Mg^{27} and Na^{24}, which were created in $Al^{27}(n, p)Mg^{27}$ and $Al^{27}(n, \alpha)Na^{24}$ reactions. The half lives of residual nuclei must be sufficiently long, in our technique, to allow the detector to be moved from the neutron flux to the gamma-ray counter. Our gamma-ray measurements have benefited from improvements in the low-background counting facility.[2]

The relation between detector activity, cross section, and neutron flux may be expressed as

$$A_i' = \int_0^\infty \phi(E)\, \sigma_i(E)\, dE, \qquad (1)$$

where A' = detector saturation activity or disintegration rate per target nucleus in sec^{-1},

$\phi(E)$ = neutron flux in $cm^{-2}\ sec^{-1}\ MeV^{-1}$,

$\sigma(E)$ = reaction cross section in cm^2,

E = neutron energy in MeV,

i = subscript identifying the reaction and residual nucleus.

There is one such equation for each reaction observed. A number of reactions form a set of integral equations which, under favorable conditions, may be solved for the unknown flux. Our previous solution method was a matrix inversion in which the form of $\phi(E)$ was assumed, and numerical values of $\phi(E)$ were found. This solution, when substituted back into the equation, reproduced exactly the activities, A_i. In cases where the original activity measurements contain substantial experimental errors, the flux solution may become unstable and produce negative values of $\phi(E)$, which are meaningless. We encountered this difficulty and substituted a solution method which solves by iteration, using only positive trial fluxes, and seeks to produce a set of calculated activities, based on the trial flux, which best fit the measured set of activities.

It was desirable to incorporate recent experimental threshold reaction cross sections (excitation functions) in the method. Our previous calculations of reaction cross sections did not show satisfactory agreement with recently published experimental data. The calculated cross sections were discarded in favor of experimental data.

II. MEASUREMENT OF DISINTEGRATION RATE

A. Counting Equipment

The counting equipment is similar to that in our earlier report on threshold detectors.[1] A single 4-in. -diam by 2-in. -thick NaI(Tl) scintillation crystal is coupled to a DuMont type 6363 photomultiplier (PM) tube. The crystal and PM tube are located in a new large, low-activity concrete cave.[2] Inside the cave a smaller 2-in. -thick lead shield surrounds the crystal and PM tube. Within the γ-ray energy interval 0.080 to 2.080 MeV the background count rate is 141.6 counts/min and is quite constant. The previous setup used a second crystal for continuous background measurement, and this crystal is no longer necessary.

A Penco PA-4 100-channel differential pulse-height analyzer (PHA) is used to analyze and store the γ-ray data. Gain is set to cover the energy interval 0.080 to 2.080 MeV in 100 channels, each 20-keV wide. Stored PHA data is tabulated on a Victor printer adding machine and the counts/channel vs channel number are simultaneously plotted on a Mosely Autograf.

B. Gamma-Ray Spectrum Analysis

1. Photopeak Analysis

Our method of γ-ray spectrum analysis is essentially the same as previously reported and is briefly outlined here.[1] Our method is a variation of spectrum stripping. Figure 1 shows one of our measured γ-ray spectra from an Al detector. Data points are shown as dots. The prominent peak near channel 60 identifies Na^{22}. The smaller peak near channel 86 represents a sum peak for scintillations from the annihilation γ ray and the 1.28-MeV γ ray in coincidence. It is of no interest in this analysis. Figure 1 also shows this spectrum separated into its components. We are interested in calculating the photopeak area in counts/sec. Analysis proceeds as follows:

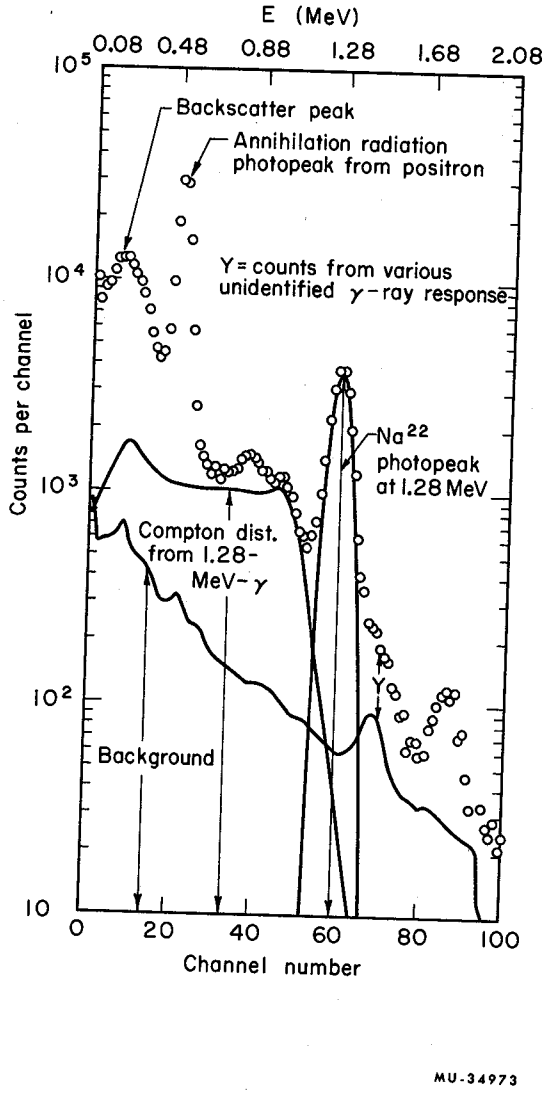

Fig. 1. Gamma-ray spectrum including Na^{22} and its components.

(a) Background is subtracted from the spectrum.

(b) The response of unidentified gamma rays of higher energy than the photopeak of interest elevates the peak. A constant quantity, Y, an estimate of this response, is subtracted from the spectrum.

(c) Based on the position and height of the photopeak maximum the Compton distribution is found from a library of such functions and subtracted from the spectrum.

(d) What remains, in principle, is the photopeak only. Aside from statistical error or errors in the quantities subtracted (a, b, and c above), the photopeak is Gaussian in shape. This remaining data is fitted to a Gaussian curve by a nonlinear least-squares technique which selects best values of photopeak area, variance, and mean (position of peak maximum).

(e) Photopeak area is the number of counts in the peak per time. Corrections are made for PHA block time, γ-ray self-absorption in the detector, branching ratio for the γ ray observed, and the ratio of counts in the peak to γ rays emitted by the activated detector. The result is the disintegration rate of the isotope of interest in the detector. The calculation is coded in FORTRAN for the IBM 7090 computer as a main program titled SUPER-3 and 15 subroutines.

2. Least-Squares Analysis

Our method of γ-ray analysis uses data only from the photopeak, which is 5 to 15 channels wide out of the 100 channels of data. A newer method currently in great favor is least-squares analysis,[3,4] which uses data from most of the spectrum. This method assembles a composite spectrum which is the sum of individual spectra of gamma rays of known radioisotopes. The heights (which are proportional to the activities) of the individual spectra are adjusted to minimize the sum of the squares of the differences, channel by channel, between the composite spectrum and the experimental spectrum of unknown composition.

Least-squares analysis should be a more accurate method than photopeak analysis. There are several practical reasons why this has not been attempted here. Many of the γ-ray spectra we have analyzed to date were very complex, being the result of exposing detectors to particle radiation whose energy spectrum reached very high energies (for example, the 6.2-BeV Bevatron). High-energy particle radiation can produce very many different radionuclides. Least-squares analysis requires a library of γ-ray spectra, representing each radionuclide likely to be encountered. Further the spectrum of a single radionuclide is seen to be different with different detector materials or different detector thicknesses. (All our detectors are "thick" sources, between 1/32 and 1 in.). For our use to date, applying least-squares analysis would be a monumental task. Where threshold detectors are standardized to several materials, each of a standard thickness, and exposed to particle radiation not having a significant ultra-high-energy component, application of least-squares gamma analysis should be practical and advantageous.

III. THRESHOLD DETECTORS

A. General Requirements

After some experience, the following criteria guide our selection of threshold detectors:

a. The Q value* for the reaction must be negative or, if not, there must be an effective energy threshold, so that neutrons below that energy do not initiate the reaction.

b. The material must be available in sufficient purity that activation of impurities does not obscure the reaction of interest.

c. The material must be safe to use and reasonably inexpensive.

d. The residual nucleus must be radioactive and emit a γ ray with an identifiable photopeak.

e. The half life of the residual nucleus must be of a convenient length. The shortest half life we have positively observed is 9.5 min for Mg^{27}. The longest is 5.27 y for Co^{60} after about one year following irradiation. It is preferable to have half lives between 1 h and 70 days.

f. The reaction cross section must be an experimentally known function of neutron energy. This last criterion largely limits our choice to (n, p), (n, α), and (n, 2n) reactions. Other experimenters have also used (n, n') reactions.[5, 6]

Our previous study led us to calculate cross sections by using the continuum model of the nucleus.[1,7,8] This was largely because of an absence of sufficient experimental data. Recent experimental data have begun to fill in energy gaps and improve resolution of a number of reactions. Figures 2 and 3 show examples of relatively good and

---

*The Q value for the reaction X(a, b)Y is defined as the energy equivalent of the mass difference between the input components, X plus a, and the reaction products, b plus Y.

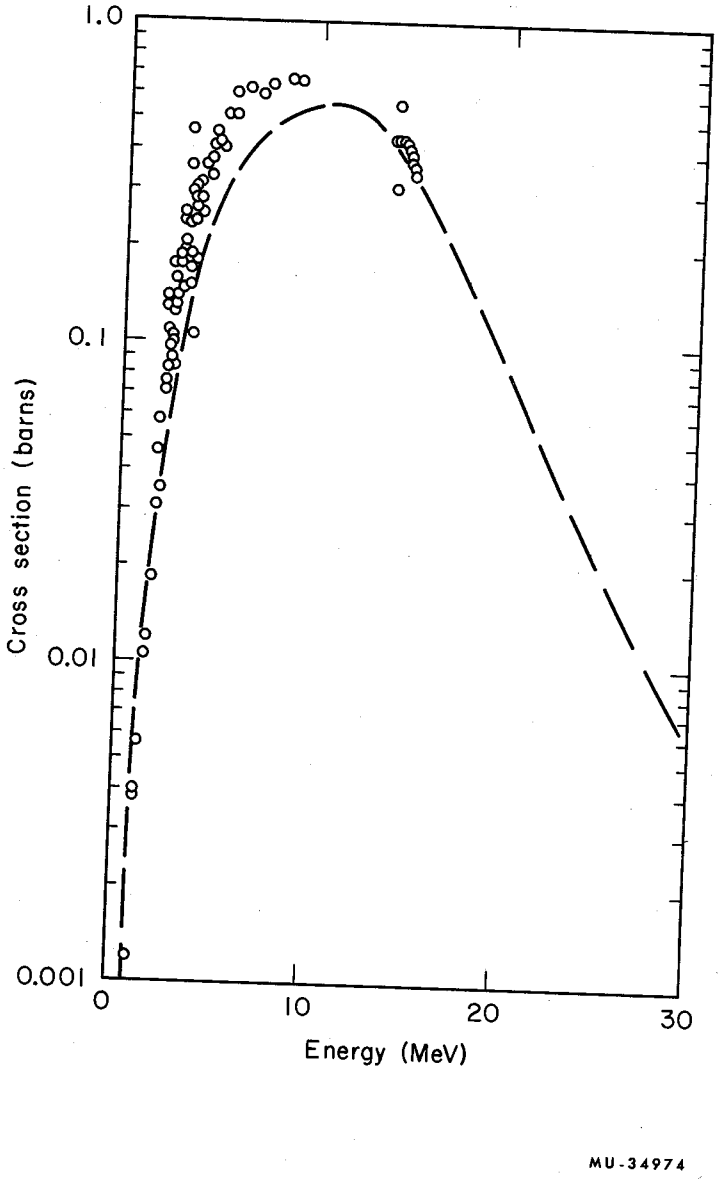

Fig. 2. Cross sections vs energy for $Ni^{58}(n, p)Co^{58}$ The dashed line shows the result of the continuum-theory calculation.

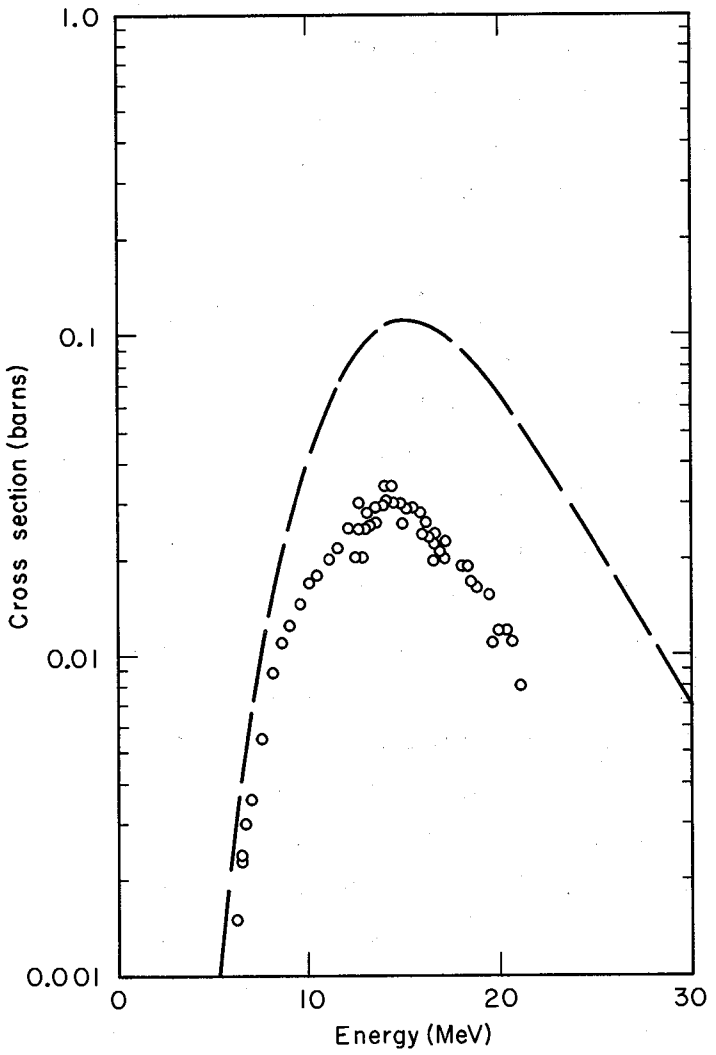

Fig. 3. Cross section vs energy for $Co^{59}(n, \alpha)Mn^{56}$. The dashed line shows the result of the continuum-theory calculation.

poor agreement, respectively, between experimental measurements and our calculated cross sections. Experimental data is indicated by dots, and no attempt is made to identify experimenters, as the data comes from many sources.[9-33] More refined continuum-theory calculations show better agreement but are still considered inadequate for our requirements.[20,21,24,25,28]

B. Useful Reactions and Cross Sections

Table I lists reactions which were found useful in our experiments, and some of their properties. Table II lists a number of other reactions of interest in future experiments, for which experimental cross sections are determined or are being determined.[34] These lists do not exhaust all possibilities but contain a variety of reactions which should satisfy many requirements. Figures 4 through 13 show experimental-cross-section measurements (dots) taken from the literature and excitation curves (solid lines) derived from these data. The excitation function is a continuous function describing the variation of the reaction-cross section with energy. We have approximated excitation functions by smooth-drawn curves through the experimental points. Increased weight was given to newer data. Very little experimental data exists beyond 21 MeV. Between the last data points and 30 MeV, the excitation curves are extrapolated. The shape drawn in this region is partly inspired by proton cross sections at high energies (see Figs. 23-27 of this report).

All detectors used in our experiments were in naturally occurring isotopic abundances. As we intend to solve neutron spectra up to 30 MeV and to correct for activation by higher-energy neutrons, we must account for the several isotopes producing the same residual nucleus through different reactions. For example, in natural nickel, neutrons may produce Co^{58} in a variety of reactions:

Isotopic abundance (%)	Reaction	Threshold energy (MeV)
67.8	$Ni^{58}(n, p)Co^{58}$	0.4
26.2	$Ni^{60}(n, t)Co^{58}$	11.7

Similarly neutrons on Ni^{61}, and Ni^{64} can produce Co^{58}. Excitation functions represented in this report include reactions induced in all natural isotopes. Experimental measurements of cross sections are often made with natural elements, so this is not a serious problem.

As an example, the excitation curve for Fig. 4, labeled Ni^{58} (n, p) Co^{58}, is actually intended to represent the cross section for Co^{58} production in natural nickel per Ni^{58} nucleus.

Table I. Threshold detectors.

Reaction	Theoretical[a] threshold (MeV)	Effective[a] threshold (MeV)	Half life of residual nucleus	Form of detector
$Ni^{58}(n, p)Co^{58}$	-0.4	1.2	71 days	4-in. metal disc
$Al^{27}(n, p)Mg^{27}$	1.8	2.7	9.5 min	4-in. metal disc
$Co^{59}(n, \alpha)Mn^{56}$	-0.3	5.3	2.58 h	4-in. metal disc
$Fe^{56}(n, p)Mn^{56}$	2.9	5.0	2.58 h	4-in. metal disc
$Ti^{48}(n, p)Sc^{48}$	3.2	5.2	44.0 h	4-in. metal disc
$Mg^{24}(n, p)Na^{24}$	4.7	6.1	15.0 h	4-in. metal disc
$Al^{27}(n, \alpha)Na^{24}$	3.1	5.9	15.0 h	4-in. metal disc
$I^{127}(n, 2n)I^{126}$	9.3	9.4	13.2 days	Boxed crystals
$Co^{59}(n, 2n)Co^{58}$	10.2	10.8	71 days	4-in. metal disc
$Ni^{58}(n, 2n)Ni^{57}$	11.8	12.5	36 h	4-in. metal disc

[a] The theoretical threshold is calculated as $-Q \times \frac{1 + M}{M}$, where Q is the Q value for the reaction and M is the mass number of the target nucleus. The effective threshold is the energy at which the cross section is 1/100 of its peak value.

Table II. Additional threshold reactions

Reactions	Theoretical threshold (MeV)	Half life of residual nucleus
Cu^{64}(n, p)Cu^{64}	-0.2	12.9 hr
Fe^{59}(n, p)Fe^{59}	0.8	45 days
V^{52}(n, p)V^{52}	3.1	3.77 min
V^{52}(n, α)V^{52}	0.6	3.77 min
Sc^{48}(n, α)Sc^{48}	1.6	44.0 h
Tl^{203}(n, 2n)Tl^{202}	8.8	12.0 days
Sb^{121}(n, 2n)$Sb^{120\ g}$	9.3	16 min
Cu^{63}(n, 2n)Cu^{62}	10.6	9.9 min
Cu^{65}(n, 2n)Cu^{64}	10.1	12.9 h
Sc^{45}(n, 2n)$Sc^{44\ m}$	11.6	2.4 days
Na^{23}(n, 2n)Na^{22}	12.9	2.6 y
F^{19}(n, 2n)F^{18}	11.0	1.87 h
Zn^{64}(n, 2n)Zn^{63}	11.8	38 min
Fe^{54}(n, 2n)Fe^{53}	13.6	9.0 min
P^{31}(n, 2n)P^{30}	12.7	2.55 min
In^{115}(n, 2n)$In^{114\ m}$	9.1	50.0 days
As^{75}(n, 2n)As^{74}	10.4	18 days
Au^{197}(n, 2n)$Au^{196\ g}$	8.1	6.1 days
C^{12}(n, 2n)C^{11}	20.3	20.4 min
Al^{28}(n, p)Al^{28}	3.99	2.3 min
Ni^{65}(n, p)Ni^{65}	1.3	2.65 h
In^{115}(n, n')$In^{115\ m}$	0.2	4.6 h
Rh^{103}(n, n')$Rh^{103\ m}$	0.04	54 min
Al^{27}(n, α)Al^{28}	2.0	2.3 min
Mo^{92}(n, 2n)Mo^{91}	13.3	16 min

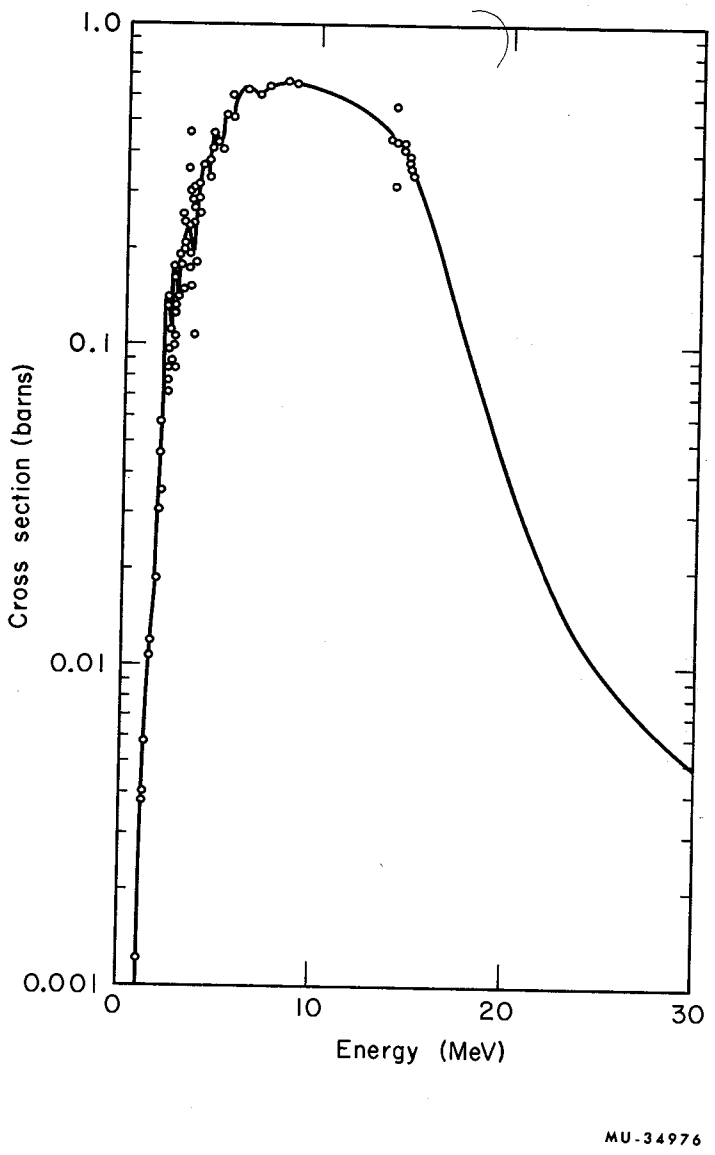

Fig. 4. Excitation function for $Ni^{58}(n, p)Co^{58}$.

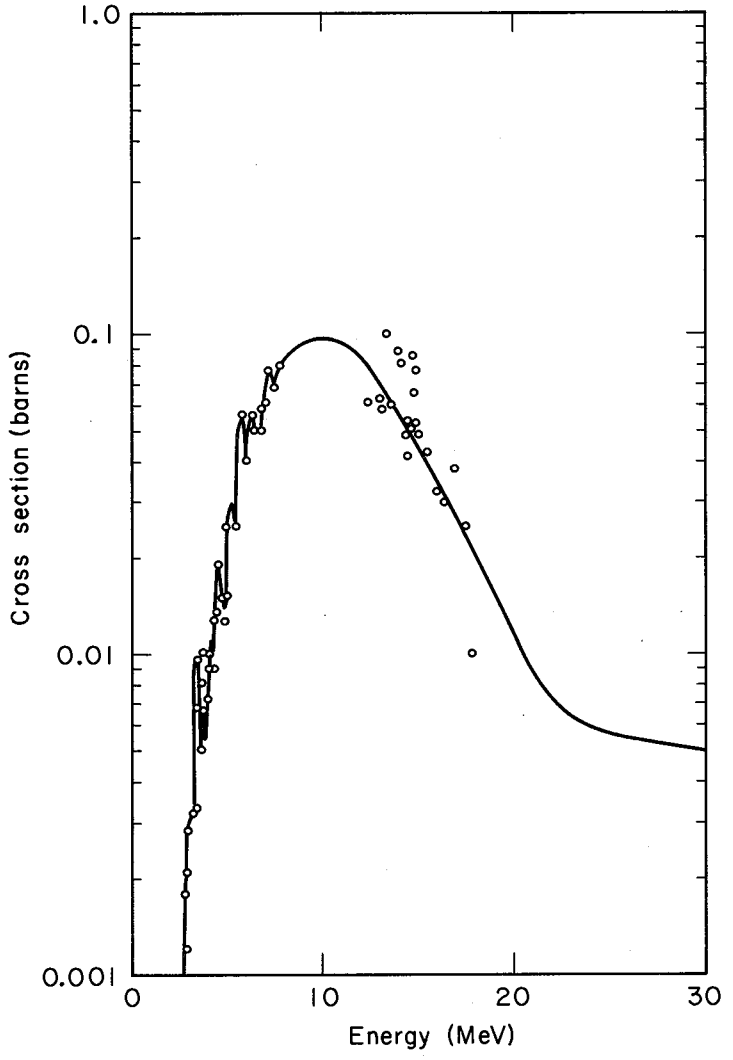

Fig. 5. Excitation function for $Al^{27}(n, p)Mg^{27}$.

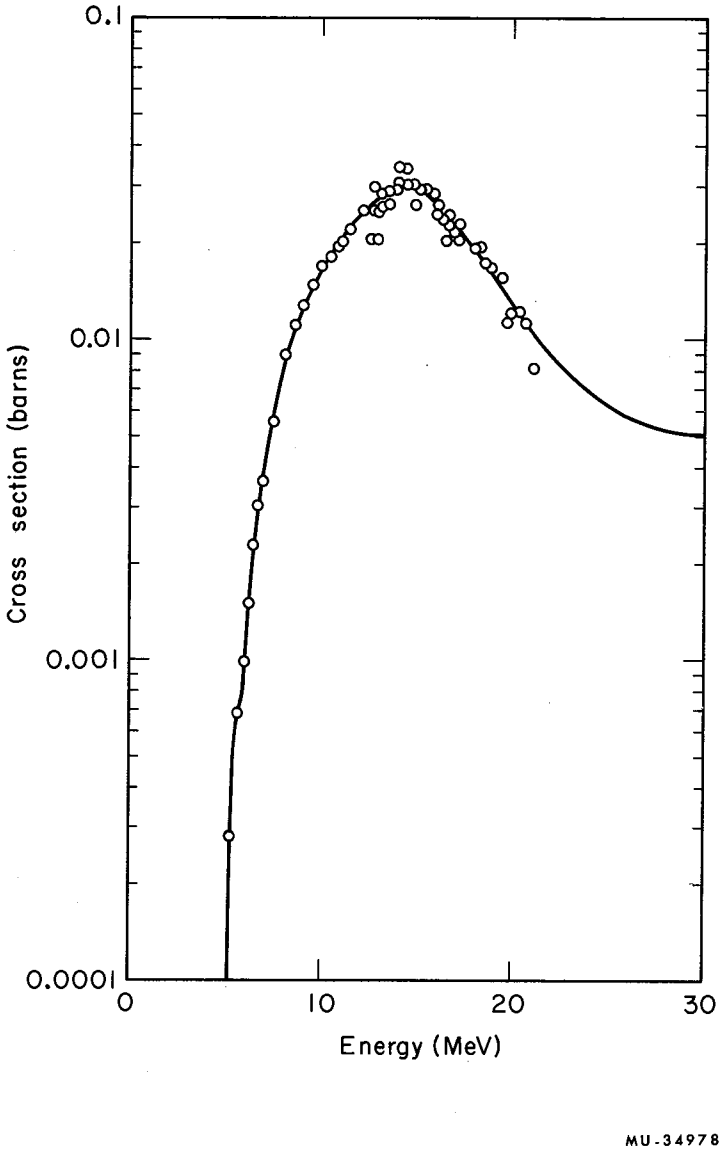

Fig. 6. Excitation function for $Co^{59}(n, \alpha)Mn^{56}$.

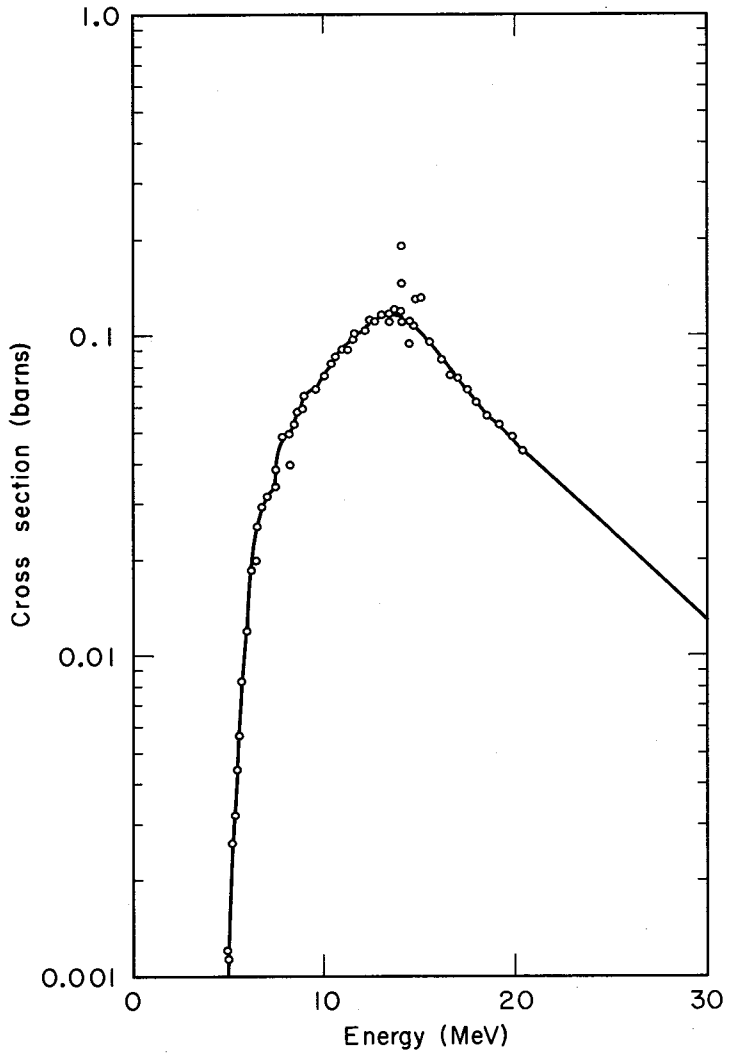

Fig. 7. Excitation function for $Fe^{56}(n, p)Mn^{56}$.

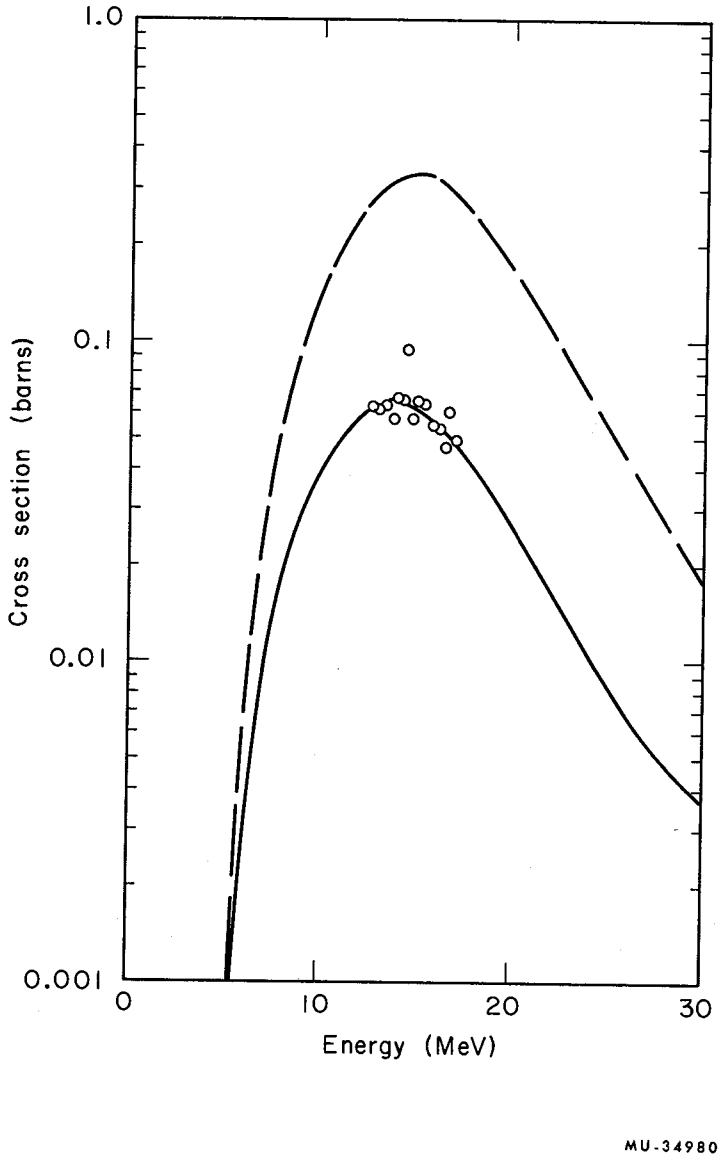

Fig. 8. Excitation function for $Ti^{48}(n, p)Sc^{48}$.

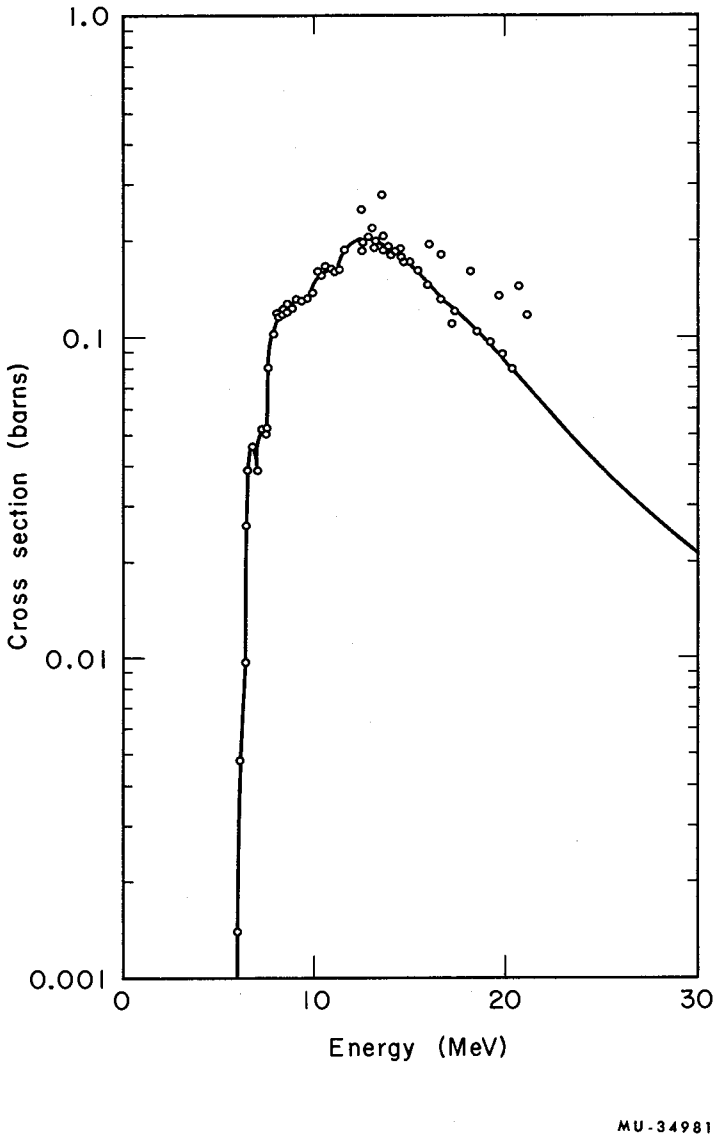

Fig. 9. Excitation function for $Mg^{24}(n, p)Na^{24}$.

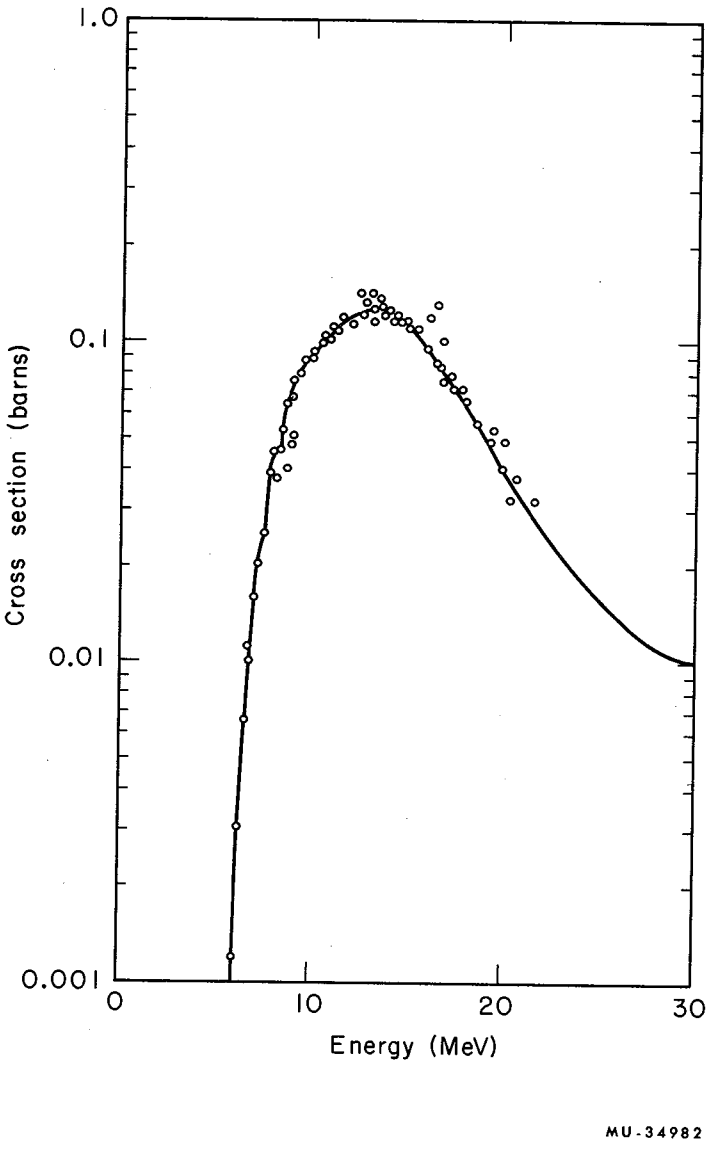

Fig. 10. Excitation function for $Al^{27}(n, \alpha)Na^{24}$.

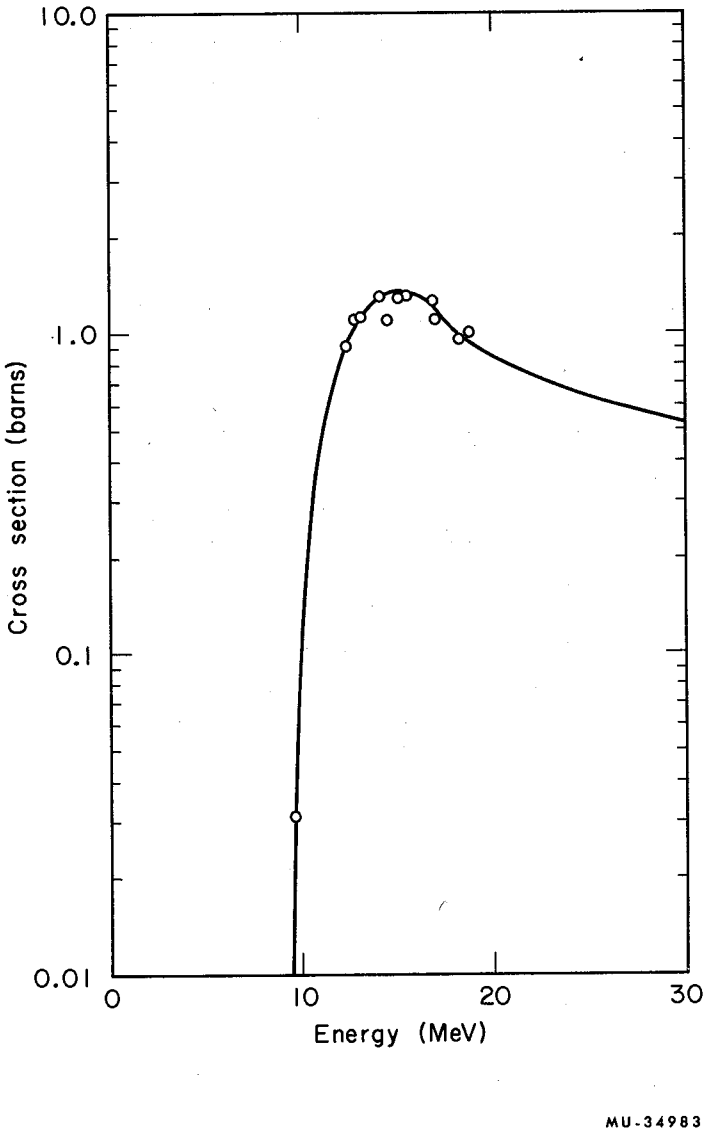

Fig. 11. Excitation function for $I^{127}(n, 2n)I^{126}$.

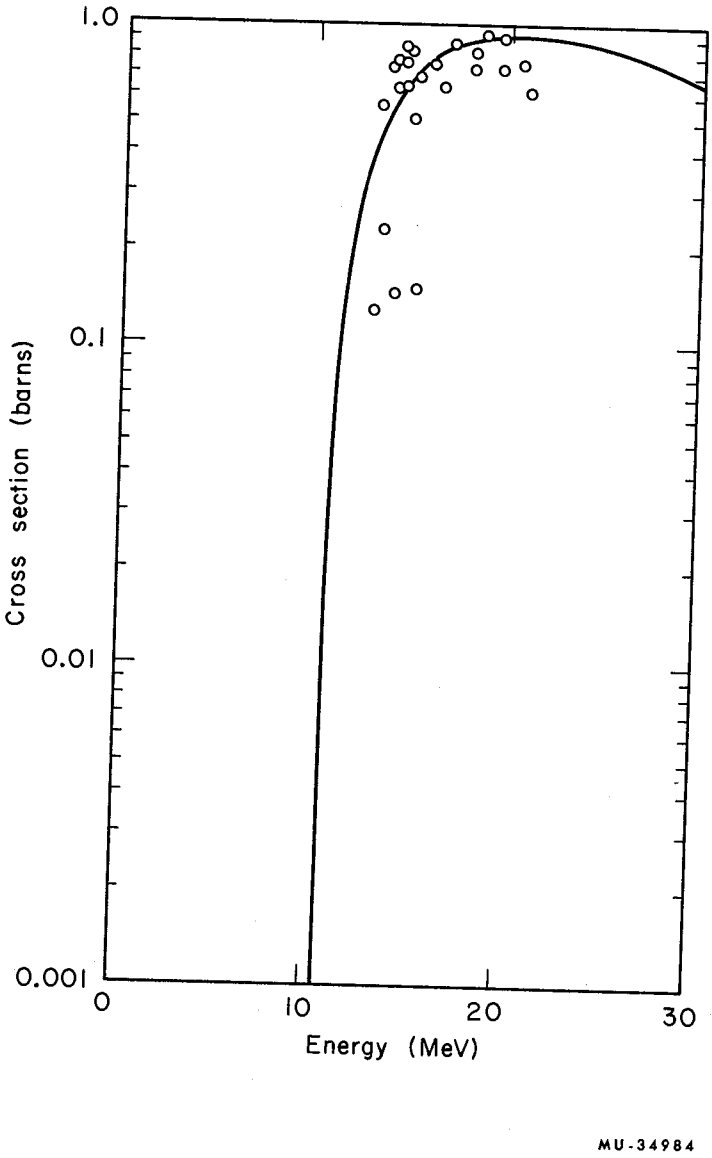

Fig. 12. Excitation function for $Co^{59}(n, 2n)Co^{58}$.

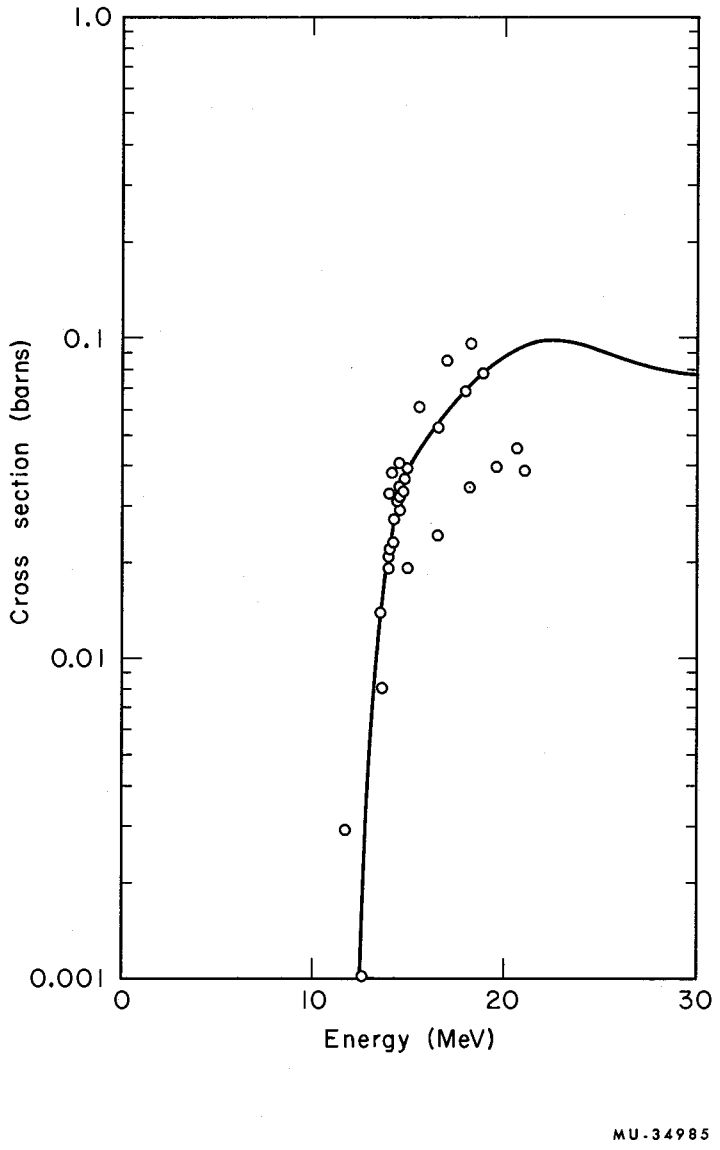

Fig. 13. Excitation function for $Ni^{58}(n, 2n)Ni^{57}$.

IV. NEUTRON-ENERGY SPECTRUM

A. Basic Relationships

The measured detector activity may be reduced to saturation activity (see Appendix A) and this, in turn, related to cross section and neutron flux by

$$A_i' = \int_0^\infty \phi(E)\, \sigma_i(E)\, dE, \tag{2}$$

where A_i' = detector saturation activity or disintegration rate per target nucleus in sec^{-1},

$\phi(E)$ = neutron flux in $cm^{-2}\ sec^{-1}\ MeV^{-1}$,

$\sigma(E)$ = reaction cross section in cm^2,

E = neutron energy in MeV, and

i = subscript identifying the reaction and residual nucleus.

There is one such equation for each reaction observed. We wish to determine the neutron spectrum below 30 MeV, so the set of equations (2) is rewritten

$$A_i' = \int_0^{30} \phi(E)\, \sigma_i(E)\, dE + \int_{30}^\infty \phi(E)\, \sigma_i(E)\, dE \tag{3}$$

and

$$A_i' = A_{30_i} + A_{max_i}. \tag{4}$$

Here we assume A_{max_i} is a relatively small part of A_i' and can be estimated separately (see paragraph V.B.1). Then we wish to solve the following set for $\phi(E)$:

$$A_{30_i} = \int_0^{30} \phi(E)\, \sigma_i(E)\, dE. \tag{5}$$

Equation (5) is a linear integral equation, called a Fredholm equation of the first kind. General discussion of its solution may be found elsewhere.[35] The following is a discussion of several practical solution methods to our particular problem.

B. Average Flux

As an introduction, assume that we will solve for the average flux in the interval 0 to 30 MeV. Any one of the set of equations (5) is sufficient for this purpose. Rearranging

$$A_{30_m} = \int_0^{30} \phi(E)\ \sigma_m(E)\ dE = \phi_A x \int_0^{30} \sigma_m(E)\, dE, \qquad (6)$$

we have

$$\phi_A = \frac{A_{30_m}}{\int_0^{30} \sigma_m(E)\, dE}, \qquad (7)$$

where ϕ_A is the average flux in $cm^{-2}\ sec^{-1}\ MeV^{-1}$. However, the value of ϕ_A calculated will depend on the reaction chosen, as illustrated in Fig. 14.

Figure 15 illustrates that the average-flux calculation may be refined by defining an energy range over which the cross section is most effective. The average flux calculated by Eq. (7) is limited to the range over which that cross section is effective. Using a number of detectors in this manner, one might make a crude estimate of a spectrum. A slightly more elegant method is considered next.

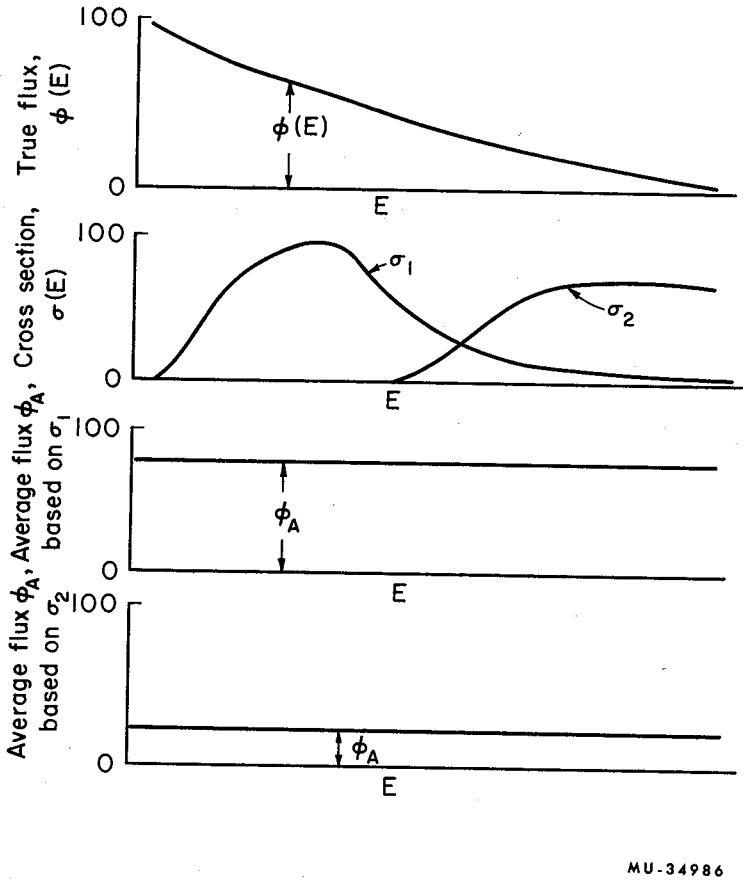

Fig. 14. Average flux calculation.

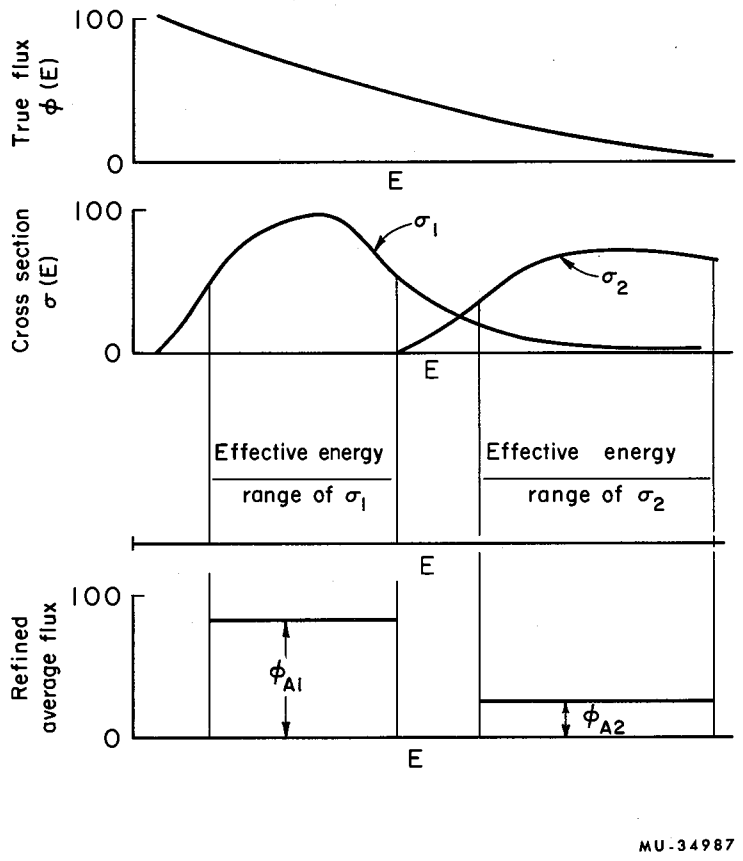

Fig. 15. Refined average flux calculation.

C. Step-Function Approximation

In this method the flux spectrum is assumed to have the form of a number of level steps. See Fig. 16. The solution of this method is the calculation of the level of each step.

1. Matrix Inversion

For the case where the number of flux steps, n, is equal to the number of reactions, and each reaction is unique or has a unique cross section shape, the basic equation (5) relating activity, flux, and cross section may be written

$$A_{30_m} = \int_0^{30} \phi(E)\,\sigma_m(E)dE = \int_0^{E_1} \phi(E)\,\sigma_m(E)dE + \int_{E_1}^{E_2} \phi(E)\,\sigma_m(E)\,dE$$

$$+ \int_{E_2}^{E_3} \phi(E)\,\sigma_m(E)\,dE + \cdots + \int_{E_{n-1}}^{30} \phi(E)\,\sigma_m(E)\,dE$$

$$= \phi_1 \int_0^{E_1} \sigma_m(E)\,dE + \phi_2 \int_{E_1}^{E_2} \sigma_m(E)\,dE$$

$$+ \phi_3 \int_{E_2}^{E_3} \sigma_m(E)\,dE + \cdots + \phi_n \int_{E_{n-1}}^{30} \sigma_m(E)\,dE$$

$$= \phi_1 I_{m_1} + \phi_2 I_{m_2} + \phi_3 I_{m_3} + \cdots + \phi_n I_{mn}$$

and

$$A_{30_m} = \sum_{j=1}^{n} \phi_j I_{m_j} . \qquad (8)$$

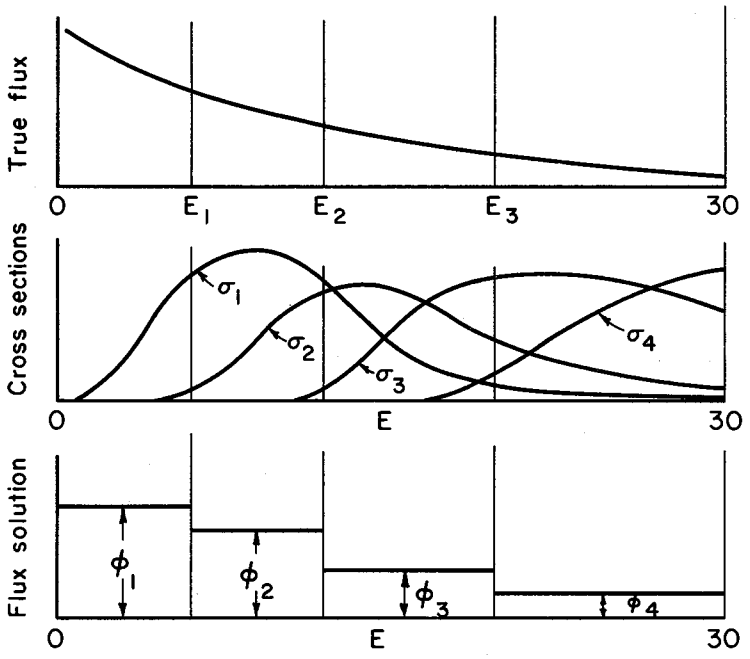

Fig. 16. Step-function approximation of flux.

To simplify notation, we define

$$I_{m_j} = \int_{E_{j-1}}^{E_j} \sigma_m(E)\, dE. \tag{9}$$

In matrix notation, Eq. (6) may be written

$$[A_{30}] = [\phi] \quad [I], \tag{10}$$

and the solution is

$$[\phi] = [I]^{-1} \quad [A_{30}].$$

This problem is simply to solve n linear algebraic equations in n unknowns. It is straightforward except that care is required in choosing the energy array or location of energy steps between 0 and 30 MeV. These steps should be chosen to maximize the absolute value of determinant [I], in order to insure accuracy in its inversion, $[I]^{-1}$. A full discussion of this feature is found in Ringle's report.[1]

A computer program has been written to select the best energy array from a number of possibilities and to solve for the step-function flux. Tests of this program have been constructed in which the "true" flux is chosen and the activities calculated from equation set (5). Such a test of the program is to solve for the flux steps, using these calculated activities and the known cross sections. Our tests demonstrate a program that satisfactorily reproduces the trial fluxes. Examples of such tests may be seen in Ringle's report.[1]

Our application of this method to experiments demonstrates a practical difficulty. In almost every case, one or more of the flux steps is negative and comparable in magnitude to the positive steps. The explanation is that the activities, A_i', are measured quantities and subject to experimental error. If the true flux and cross sections were known exactly, calculated activities would not exactly match measured

activities because of experimental error. In order to reproduce measured activities exactly, the calculated flux often takes on negative values. This difficulty has been of such magnitude that matrix inversion has been abandoned as a practical method.

(9)

2. Least-Squares Fitting

In this method, the number of flux steps, n, is chosen and need not equal the number of reactions, ℓ.

(10)

The basic relation between activity, flux, and cross section is again Eq. (8). Suppose that a set of trial values are selected for the flux steps. Calculated "activities" may be found from

$$B_m = \sum_{j=1}^{n} f_j I_{mj}, \tag{11}$$

where B_m = calculated activity for reaction m,

f_j = trial flux step between E_{j-1} and E_j.

The degree of misfit between measured activities, $\{A_{30_m}\}$, and calculated activities, $\{B_m\}$, may be computed as

$$D = \sum_{m=1}^{\ell} \frac{\left(A_{30_m} - B_m\right)^2}{A_{30_m}^2}. \tag{12}$$

The better the set of trial fluxes, $\{f_j\}$, is chosen, the better the calculated activities, $\{B_m\}$, match the measured activities, $\{A_{30_m}\}$, and the smaller D becomes. An unstable solution is to be avoided by choosing only positive values for trial fluxes. The problem is to minimize D with respect to n variables, $\{f_j\}$.

D. Polygonal Approximation

To obtain a flux-spectrum solution that is a continuous function, one may assume that the solution has a polygonal form, composed of straight-line segments connected at the ends (see Fig. 17). The

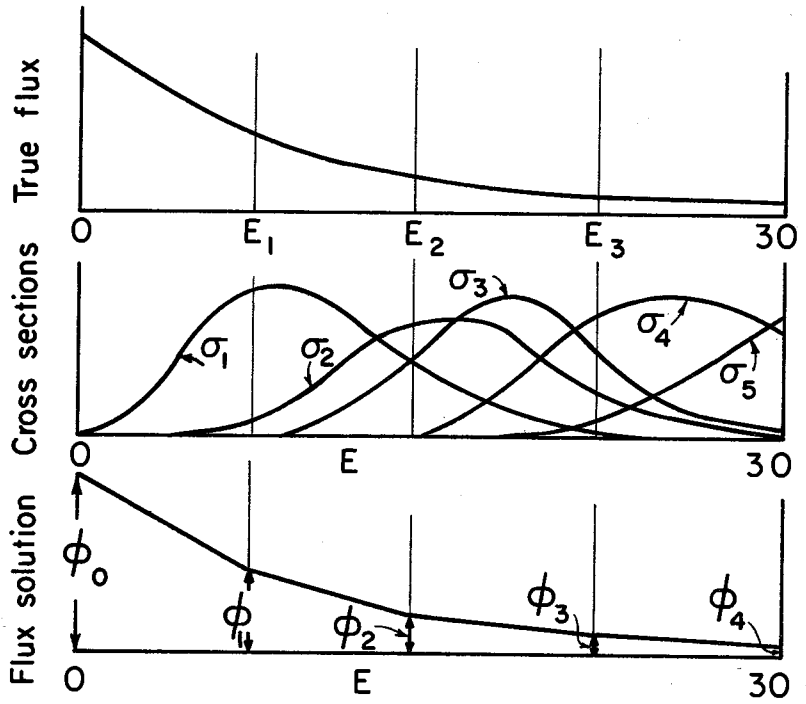

Fig. 17. Polygonal approximation of flux.

solution of this method is the calculation of the flux at each line-segment end point. Where the number of variables, ϕ_0, ϕ_1, ϕ_2, $\cdots$, is equal to the number of reactions with unique cross-section shapes, the spectrum may be solved by matrix inversion.[1] The procedure is similar to the matrix inversion previously applied to the step function and is subject to the same practical difficulty. The calculated flux oscillates between positive and negative values when the activation data contain experimental errors. Least-squares fitting of positive values again provides the solution.

The polygonal flux is assumed to have the form:

$$\phi(E) = \phi_2\left(\frac{E-E_1}{E_2-E_1}\right) + \phi_1\left(\frac{E_2-E}{E_2-E_1}\right) \tag{13}$$

for $E_1 \leq E \leq E_2$. Similarly, flux may be expressed between any other two end points. The basic equation (5) relating activity, flux, and cross section may be written

$$A_{30_m} = \int_0^{30} \phi(E)\,\sigma_m(E)\,dE = \int_0^{E_1}\left[\phi_1\left(\frac{E-E_0}{E_1-E_0}\right) + \phi_0\left(\frac{E_1-E}{E_1-E_0}\right)\right]\sigma_m(E)\,dE$$

$$+ \int_{E_1}^{E_2}\left[\phi_2\left(\frac{E-E_1}{E_2-E_1}\right) + \phi_1\left(\frac{E_2-E}{E_2-E_1}\right)\right]\sigma_m(E)\,dE + \cdots$$

$$+ \int_{E_{n-1}}^{30}\left[\phi_n\left(\frac{E-E_{n-1}}{30-E_{n-1}}\right) + \phi_{n-1}\left(\frac{30-E}{30-E_{n-1}}\right)\right]\sigma_m(E)\,dE,$$

where $n+1$ is the number of variables. This equation may be further simplified to

$$A_{30_m} = \phi_0 \left[\frac{1}{E_1 - E_0}\left(E_1 I_{m1} - J_{m1}\right)\right] + \phi_1 \left[\frac{1}{E_1 - E_0}\left(J_{m1} - E_0 I_{m1}\right) + \frac{1}{E_2 - E_1}\left(E_2 I_{m2} - J_{m2}\right)\right]$$

$$+ \phi_2 \left[\frac{1}{E_2 - E_1}\left(J_{m2} - E_1 I_{m2}\right) + \frac{1}{E_3 - E_2}\left(E_3 I_{m3} - J_{m3}\right)\right] + \cdots + \phi_n \left[\frac{1}{30 - E_{n-1}}\left(J_{mn} - E_{n-1} I_{n}\right)\right.$$

$$A_{30_m} = \sum_{j=1}^{n} \phi_j \left[\frac{1}{E_j - E_{j-1}}\left(J_{mj} - E_{j-1} I_{mj}\right)\right] + \sum_{j=0}^{n-1} \phi_j \left[\frac{1}{E_{j+1} - E_j}\left(E_{j+1} I_{m,\,j+1} - J_{m,\,j+1}\right)\right] \tag{14}$$

Notation has been simplified by defining

$$J_{mj} = \int_{E_{j-1}}^{E_j} E\, \sigma_m(E)\, dE \tag{15}$$

and by using Eq. (9) to define I_{mj}.

The number of variables, $n + 1$, is chosen and may be less than or equal to the number of reactions, ℓ. A set of trial values, $\{f_j\}$, may be selected to represent the set of flux variables, $\{\phi_j\}$. Based on the trial values, calculated "activities" may be found from

$$B_m = \sum_{j=1}^{n} f_j \left[\frac{1}{E_j - E_{j-1}}\left(J_{mj} - E_{j-1} I_{mj}\right)\right] + \sum_{j=0}^{n-1} f_j \left[\frac{1}{E_{j+1} - E_j}\left(E_{j+1} I_{m,\,j+1} - J_{m,\,j+1}\right)\right] \tag{16}$$

where B_m is the calculated activity for reaction m. Using Eq. (12) we compute and minimize the degree of misfit between measured activities, $\{A_{30_m}\}$, and calculated activities, $\{B_m\}$, by choosing better and better trial values, $\{f_j\}$. Negative flux values are avoided by choosing only positive values for the trial variables.

E. Computer Programs

Two computer programs were written to calculate flux spectra--FLUXSPOS for the step function and FLUXPPOS for the polygonal flux. Least-squares fitting of trial fluxes to minimize D [see Eq. (12)] is carried out by subroutine VARMINT.[36] These programs also calculate detector saturation activity per target nucleus caused by neutrons of less than 30 MeV; refer to Eq. (3) and the Appendix. Input data for the programs includes disintegration rate (an output of SUPER-3), count time, wait time, irradiation time, half life, detector weight, atomic weight of target element, abundance of target isotope, fraction of activation caused by neutrons below 30 MeV, neutron-energy end points, and initial trial values of flux. Calculations are done on the Lawrence Radiation Laboratory's IBM 7094 computer.

V. EXPERIMENTAL RESULTS

A. Measurement of $Be^9(d, n)B^{10}$ Neutron Spectra

Calculations of neutron-energy spectra based on measurements reported in Ringle's report[1] were repeated using our least-squares analysis.

Ringle's experiment is briefly described as follows. Threshold detectors were exposed to neutrons from the $Be^9(d, n)B^{10}$ reaction using 25- and 33-MeV deuterons from the 88-in. cyclotron at the Lawrence Radiation Laboratory. Threshold detectors were placed in a ring 28 in. from the Be target and approximately 17 deg from the target axis in the forward direction. Average deuteron-beam strengths for the bombardments were 2.37 μA for 25 MeV and 2.0 μA for 33 MeV.

We used activities resulting from $Ni^{58}(n, p)Co^{58}$, $Fe^{56}(n, p)Mn^{56}$, $Ti^{48}(n, p)Sc^{48}$, $Mg^{24}(n, p)Na^{24}$, $Al^{27}(n, \alpha)Na^{24}$, $Co^{59}(n, 2n)Co^{58}$, and $Ni^{58}(n, 2n)Ni^{57}$ reactions in recalculating neutron-energy spectra. Results of these calculations and previous measurements are shown in Figs. 18 and 19. Figure 18 demonstrates satisfactory agreement between our method and previous measurement of similar neutron spectra by others.

B. Neutron Spectra in a Thick Concrete Shield Exposed to a 6.2-BeV Proton Beam

Our technique was next applied to the neutron spectrum inside a thick concrete shield exposed to 6.2-BeV protons at the Lawrence Radiation Laboratory Bevatron. This experiment is reported elsewhere in detail.[38] Figure 20 shows a plan view of the shield, incident beam, and detector positions at which the neutron-energy spectrum has been solved. This spectrum measurement was complicated by two problems we had not encountered previously. One was that the variety of high-energy secondary particles in the shield produced many radioisotopes in the detectors compared to the few isotopes resulting from $Be^9(d, n)B^{10}$

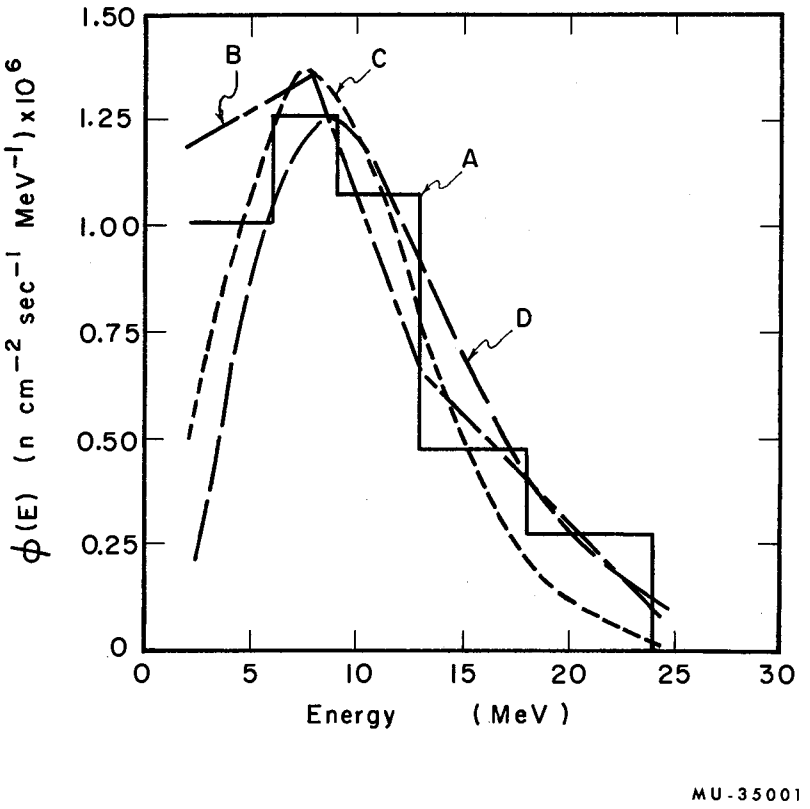

Fig. 18. Measured neutron-energy spectrum from 25-MeV deuterons on Be (17 deg from forward). Curve A has calculated by the step-function method, curve B by the polygonal method, curve C from emulsion data of Tochilin[37] for 24-MeV deuterons on Be (forward), and curve D from threshold-detector data of Heertje and Aten[6] for 26-MeV deuterons on Be (forward). The curves of Tochilin and of Heertje and Aten were normalized so that the area under the curves matches that under curve A.

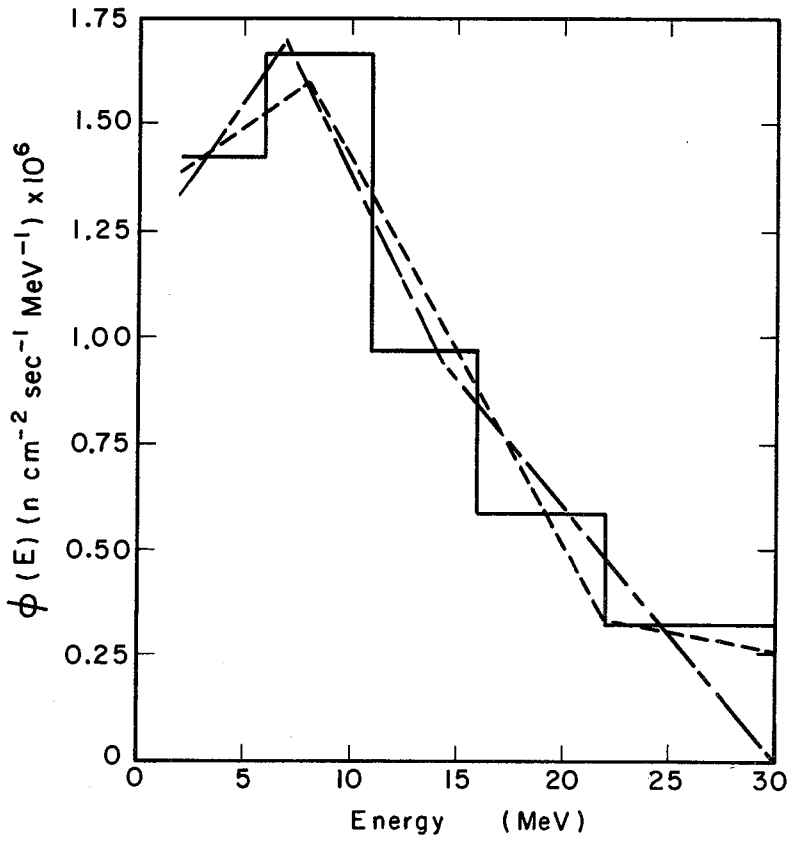

Fig. 19. Measured neutron energy spectrum from 33-MeV deuterons on Be (17 deg from forward). The two polygonal-method curves were calculated using identical data but with different energy end points.

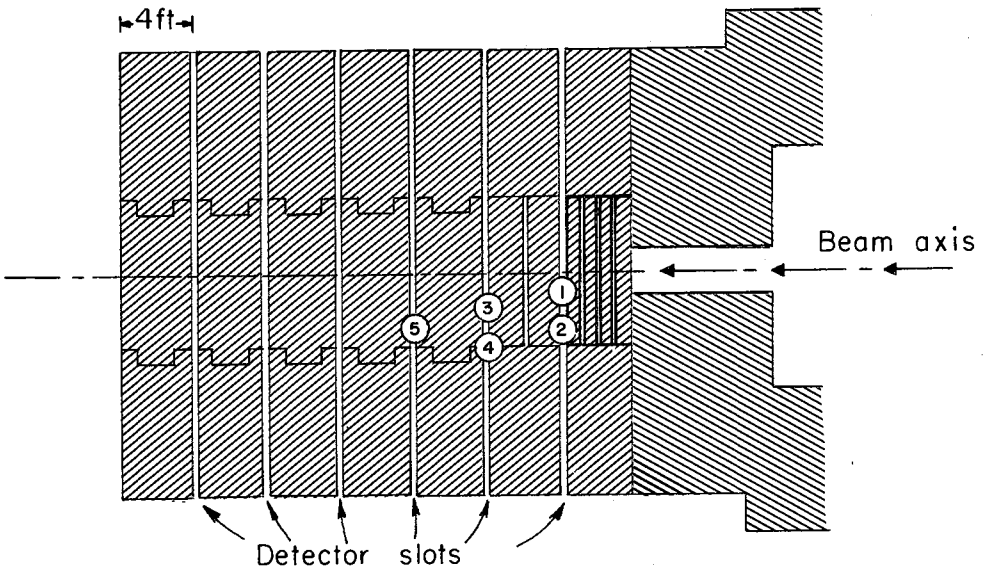

Fig. 20. Plan view of shield array showing five detector locations where energy spectrum was solved: (1) 4'-1', (2) 4'-3', (3) 8'-2', (4) 8'-4', (5) 12'-3'. Notation 4'-1' signifies 4 feet along the beam axis from the point of beam incidence and 1 foot off the beam axis.

neutron sources. Gamma-ray spectra from detectors placed in this concrete shield were very complex, and some desired reactions, $Ni^{58}(n, 2n)Ni^{57}$ for example, were obscured by radioisotopes of similar γ-ray energy. The second and more serious problem was that a significant fraction of the measured activity was caused by neutrons of energies in excess of 30 MeV, the upper limit of our spectrum solution technique.

1. Correction for High-Energy Activation

The fraction of activation caused by neutrons and other particles of energies greater than 30 MeV cannot be directly measured. Unlike the effect of cadmium on low-energy neutrons, there is no material with a large cross section which rises sharply below 30 MeV. An indirect method was used in which the shape of the neutron spectrum was estimated, and a high-energy threshold reaction used to determine the level or amplitude of that flux shape.

a. Flux-Shape Estimate. Based in part, on the Monte Carlo calculation of Metropolis et al.,[39] Moyer and Wallace[40] have calculated neutron-energy spectra for 450, 600, and 850-MeV protons incident on an extended thick object. From their number-density spectrum, n(E), a flux spectrum, v. n(E) = ϕ(E), has been calculated (see Fig. 21). For convenience in calculations, the flux spectrum is approximated by an $E^{-1/2}$ shape above 30 MeV. For $30 < E \leq 1000$ MeV the flux spectrum is assumed to be

$$\phi(E) = \phi(30)\sqrt{\frac{30}{E}},$$

and for $E > 1000$ MeV,

$$\phi(E) = 0,$$

where $\phi(30)$ is the particle flux at 30 MeV in cm^{-2}-sec^{-1}-MeV^{-1}.

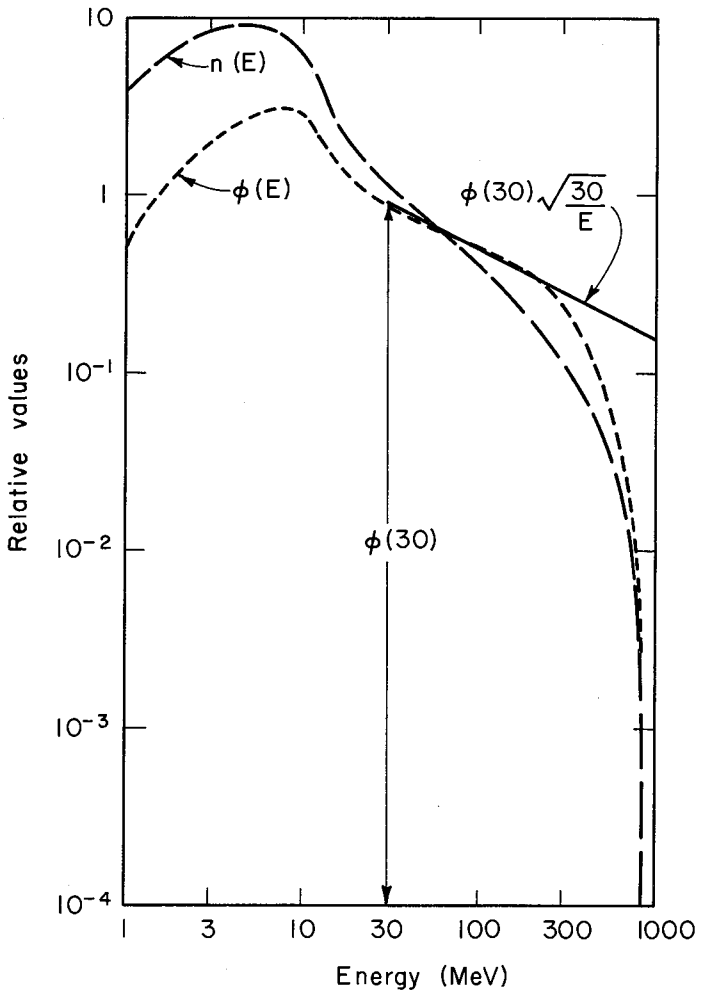

Fig. 21. Calculated neutron-energy spectra for 850-MeV protons incident on an extended thick object. The solid line is an approximation to ϕ (E).

Lacking appropriate calculations for 6.2-BeV incident protons, we have assumed that the neutron-energy spectrum has the same shape as for incident 850-MeV protons.

b. Amplitude of High-Energy Flux. With rare exceptions,[41-45] neutron-reaction cross sections have not been measured at high energies, although a number of proton-reaction cross sections are fairly well known. In general, we have assumed that at the high energies, cross sections for formation of a particular radionuclide are the same for neutrons and protons.

In polyethylene detectors placed in the concrete shield, we observed Be^7 from $C^{12}(n, \alpha 2n)\,Be^7$ and $C^{12}(p, 3p3n)\,Be^7$. The cross section for $C^{12}(p, 3p3n)\,Be^7$ is a well-determined function of energy[45,46] and is shown in Fig. 22. The threshold for this reaction is 38.5 MeV. Under our assumptions, the Be^7 activity is expressed as

$$A_1' = \int_0^\infty \phi(E)\,\sigma_1(E)\,dE = \phi(30) \int_0^{1000} \sqrt{\frac{30}{E}}\,\sigma_1(E)\,dE, \qquad (17)$$

and therefore,

$$\phi(30) = \frac{A_1'}{\int_0^{1000} \sqrt{\frac{30}{E}}\,\sigma_1(E)dE}\,.$$

Having calculated $\phi(30)$, we use this same procedure to calculate the activation of other detectors caused by neutrons of energies above 30 MeV.

c. High-Energy Cross Sections. Figures 23 through 27 show neutron cross sections below 30 MeV and proton cross sections above 30 MeV. Sources of experimental proton cross sections are numerous,[45-56] and are not identified in the following figures. The smooth curves were drawn to define $\sigma(E)$ used in the calculation of

$$\int_0^{1000} \sqrt{\frac{30}{E}}\,\sigma(E)\,dE.$$

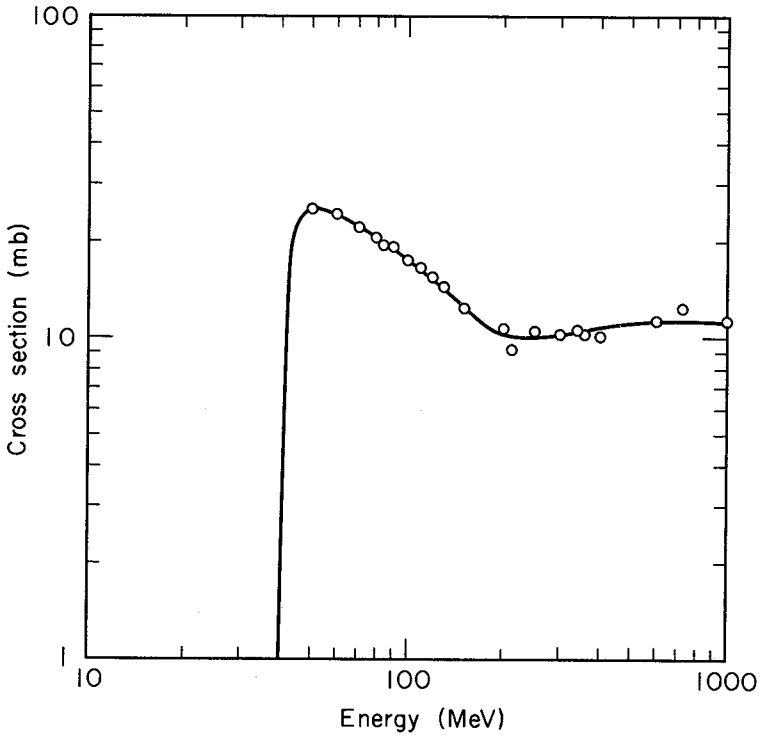

Fig. 22. Excitation function for $C^{12}(p, 3p3n)Be^{7}$.

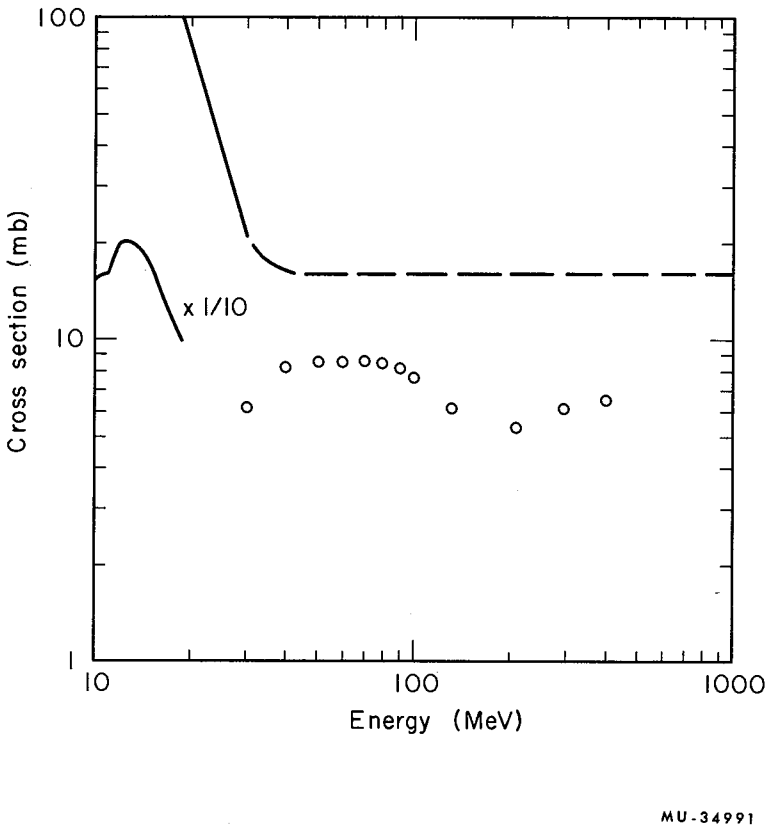

Fig. 23. Excitation function for $Mg^{24}(n, p)Na^{24}$. Data points are shown for $Mg(p, -)Na^{24}$. See text for an estimate of the high-energy cross section.

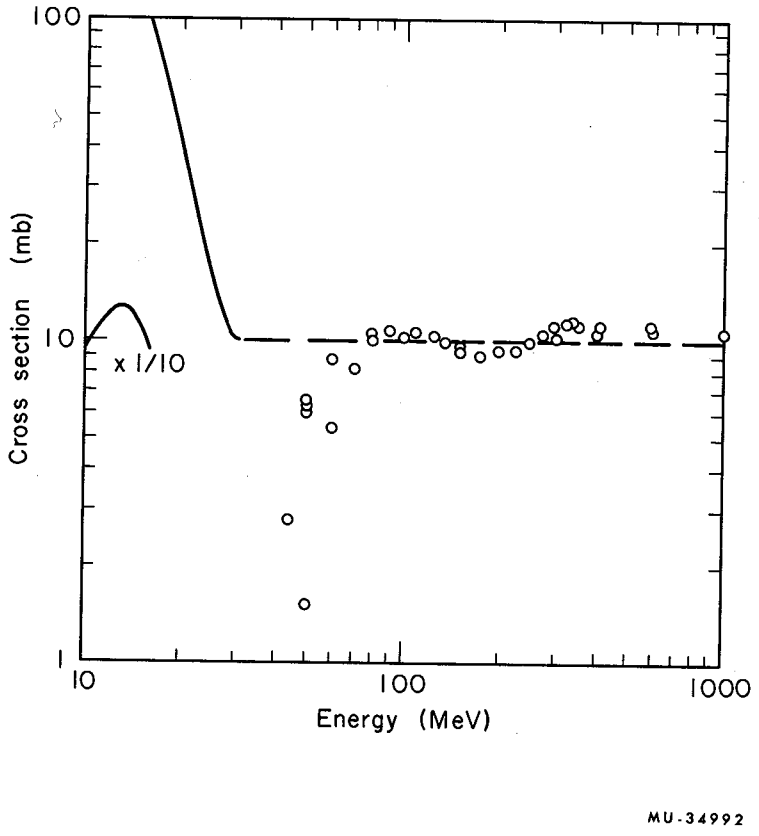

Fig. 24. Excitation function for $Al^{27}(n, \alpha)Na^{24}$. Data points are shown for $Al^{27}(p, 3pn)Na^{24}$.

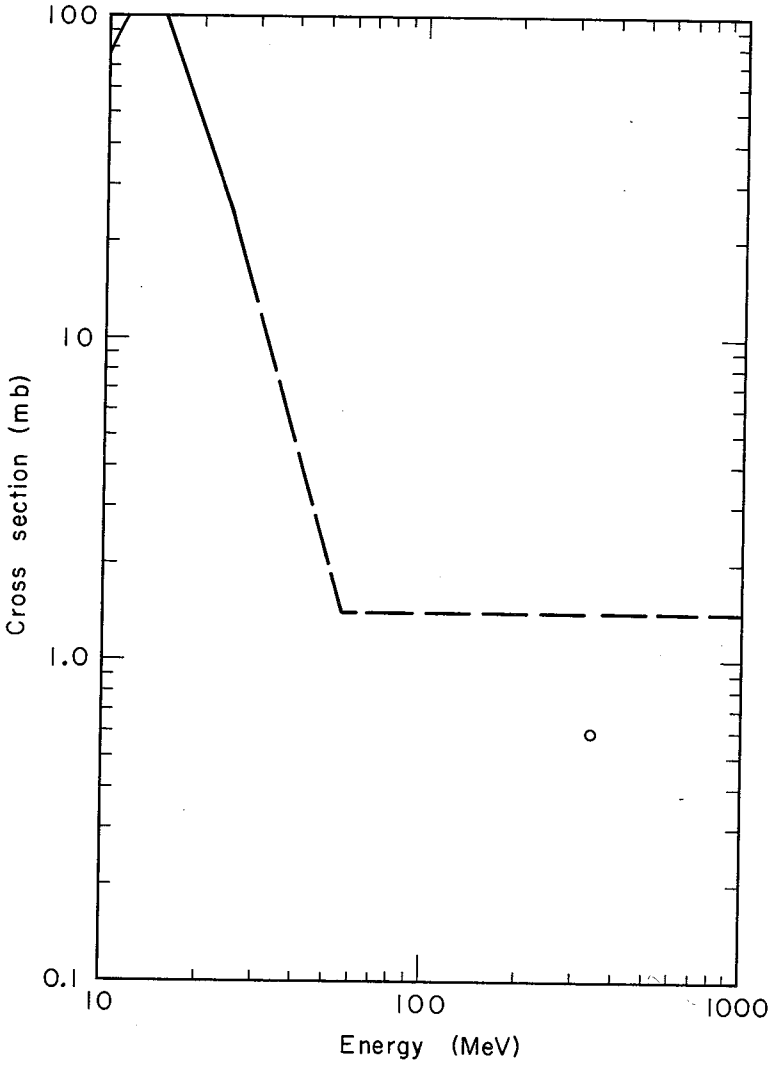

Fig. 25. Excitation function for $Fe^{56}(n, p)Mn^{56}$. A data point is shown for $Fe(p, -)Mn^{56}$. See text for an estimate of the high-energy cross section.

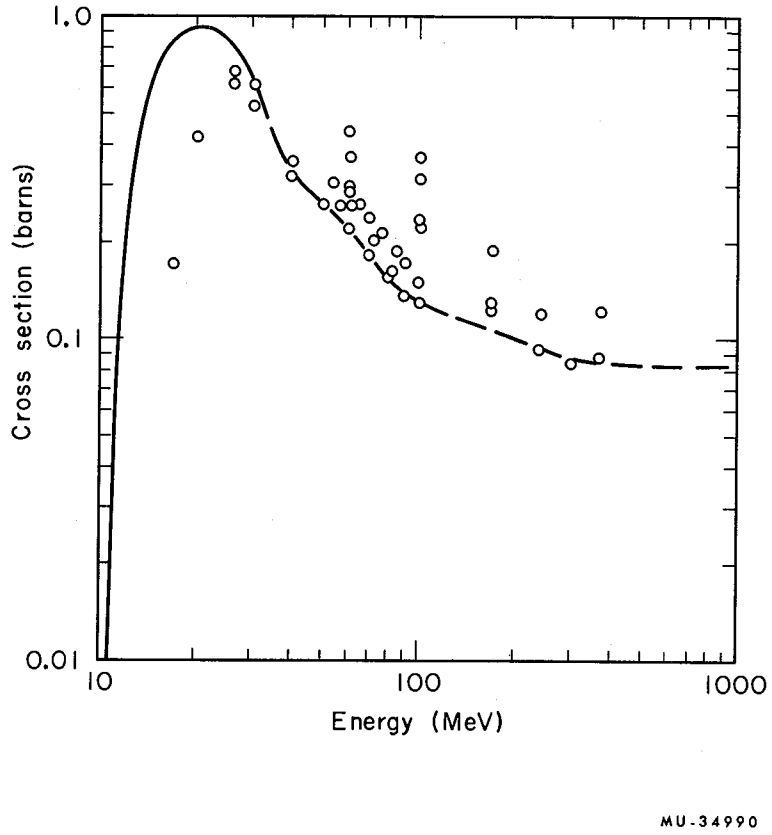

Fig. 26. Excitation function for $Co^{59}(n, 2n)Co^{58}$. Data points are shown for $Co^{59}(p, pn)Co^{58}$.

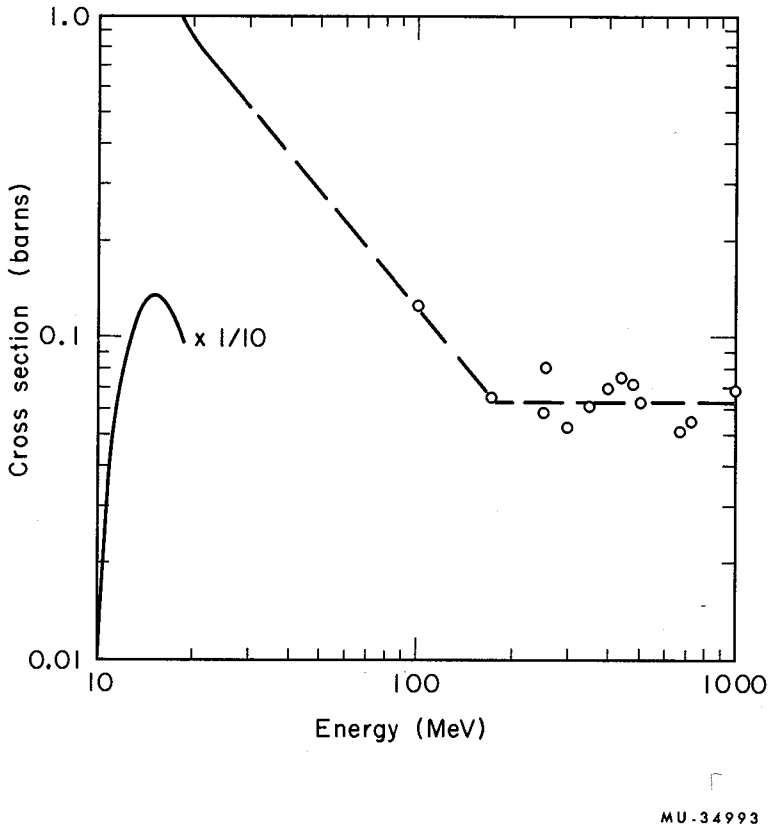

Fig. 27. Excitation function for $I^{127}(n, 2n)I^{126}$. Data points are shown for $I^{127}(p, pn)I^{126}$.

A literature search did not reveal any experimental cross-section values for Co^{58} formation by neutrons or protons above 30 MeV on nickel. The high-energy cross section was estimated as follows: At 396 MeV, the cross section for $Ni(p, pxn)Co^{56}$ is 45 mb.[58] Naturally occurring nickel has five isotopes: Ni^{58}, 67.8% abundance; Ni^{60}, 26.2%; Ni^{61}, 1.2%; Ni^{62}, 3.7%; and Ni^{64}, 1.2%. At high energy, we assume that $Ni^{58}(p, 2pn)Co^{56}$ is the predominant reaction, and that others resulting in Co^{56} [for example, $Ni^{60}(p, 2p3n)Co^{56}$] may be neglected. From this assumption it follows that the $Ni^{58}(p, 2pn)Co^{56}$ cross section is $45 \times 1000/0.678 = 66$ mb. For formation of Co^{58}, the predominant reaction at high energies is assumed to be $Ni^{60}(p,2pn)Co^{58}$, and other reactions resulting in Co^{58} are assumed to be negligible. Next we assume that the cross section for $Ni^{60}(p, 2pn)Co^{58}$ is also 66 mb. It follows that the formation cross section for Co^{58} from natural Ni (per Ni^{58} nucleus) is $66 \times 0.262/0.678 = 25$ mb. As before, we assume that the high-energy reaction cross section is the same for neutrons and protons.

Experimental high-energy cross-section data is available for $Mg(p, xn)Na^{24}$.[49,58] A plot in Fig. 23 shows that this cross section has an average value of about 6 mb above 100 MeV. Isotopic abundances in Mg are Mg^{24}, 78.7%; Mg^{25}, 10.1%; and Mg^{26}, 11.3%. Per Mg^{24} nucleus, this cross section is $6/0.787 = 7.6$. Protons may produce Na^{24} in Mg in the following reactions:

1. $Mg^{25}(p, p')Mg^{25*} \rightarrow Na^{24} + p$
2. $Mg^{26}(p, p')Mg^{26*} \rightarrow Na^{24} + p + n$
3. $Mg^{26}(p, n)\,Al^{26*} \rightarrow Na^{24} + 2p.$

Neutrons may produce Na^{24} in Mg in the following reactions:

4. $Mg^{24}(n, p)Na^{24}$
5. $Mg^{25}(n, n')Mg^{25*} \rightarrow Na^{24} + p$
6. $Mg^{25}(n, p)Na^{25*} \rightarrow Na^{24} + n$
7. $Mg^{26}(n, n')Mg^{26*} \rightarrow Na^{24} + p + n$
8. $Mg^{26}(n, p)Na^{26*} \rightarrow Na^{24} + 2n.$

Based on measurement of the cross section for $Al^{27}(n, p)Mg^{27}$ at 5.1 m at 370 MeV,[44] reaction 4 is estimated to have a cross section of 5 mb. Reactions 5 plus 7 plus 8 are assumed to have the same cross section as 1 plus 2 plus 3. To account for reaction 6 for which there is no similar proton-induced reaction, the total for numbers 5 through 8 is assumed to be $1.5 \times 7.6 = 11.4$ mb. It follows from these assumptions that the high-energy-neutron reaction cross section per Mg^{24} nucleus is $11.4 + 5 \approx 16$ mb.

There are no experimental-cross-section measurements for Mn^{56} production by high-energy neutrons on iron. The 340-MeV cross section is 0.59 mb for $Fe(p, 2pxn)Mn^{56}$ and 0.24 mb for $Fe(p, xn)Co^{56}$.[50] Naturally occurring iron has four isotopes: Fe^{54}, 5.8% abundant; Fe^{56}, 91.7%; Fe^{57}, 2.2%; and Fe^{58}, 0.3%. High-energy protons on iron may produce Mn^{56} by the reaction:

1. $Fe^{57}(p, p')Fe^{57*} \rightarrow Mn^{56} + p.$

Here Fe^{58} is neglected, being in very small quantity. High-energy neutrons may produce Mn^{56} by:

2. $Fe^{56}(n, p)Mn^{56}$
3. $Fe^{57}(n, n')Fe^{57*} \rightarrow Mn^{56} + p$
4. $Fe^{57}(n, p)Mn^{57*} \rightarrow Mn^{56} + n.$

The cross section for reaction 2 is estimated as 0.24 mb from the cross section measured for $Fe(p, xn)Co^{56}$. The cross section of reactions 3 plus 4 is estimated to be twice that of 1. From these assumptions, it follows that the high-energy-neutron cross section for Mn^{56} production, per Fe^{56} nucleus, is $2 \times 0.59 + 0.24 = 1.4$ mb.

d. Calculation of High-Energy Activation. For each location in the shield where the $C^{12}(n, \alpha 2n)Be^{7}$ reaction was observed, the calculated activation due to particles of energy greater than 30 MeV is

$$A_{max_i} = \int_{30}^{\infty} \phi(E)\sigma_i(E)dE = \phi(30) \int_{30}^{1000} \sqrt{\frac{30}{E}}\ \sigma_i(E)\, dE. \qquad (18)$$

From $A_{30_i} = A_i' - A_{max_i}$, where A_i' is measured and A_{max_i} is calculated above, we can solve the basic set of equations for $\phi(E)$ in the previous manner. Because the high-energy flux shape and cross sections are both estimates, the calculated activation, A_{max}, is subject to a large error. This error is taken to be of the order of A_{max}. For most of our reactions A_{max} was between 1 and 10% of A'; in one case, it was 23.5%.

2. Measured Spectra

Figures 28 through 32 show neutron spectra determined at a number of locations in the shield. Note that these spectra decrease with increasing energy, as expected. The high flux values below 10 MeV are consistent with emulsion measurements of Bevatron stray-neutron spectra.[59] The spacing of reaction thresholds is such that a peak in the few MeV region could not be resolved in these calculations.

At each location except 4' - 1', five reactions were used: $Ni^{58}(n, p)Co^{58}$; $Fe^{56}(n, p)Mn^{56}$; $Al^{27}(n, \alpha)Na^{24}$; $Mg^{24}(n, p)Na^{24}$; and $Co^{59}(n, 2n)Co^{58}$. At location 4' - 1', the reaction $I^{127}(n, 2n)I^{126}$ was added to these five.

3. Evaluation

Note that the spectral solutions are stable, in that they are not oscillatory. This was assured by limiting the number of variables to three, for example, when five reactions were used. Such a problem would be over-determined if solution were attempted by matrix inversion; however our least-squares technique makes an optimum selection of three flux variables to fit five activities.

If experimental activity measurements are subject to large error, as was the case in our experiment at the Bevatron, oscillatory solutions can result from our least-squares technique. Solutions can be made stable by limiting the number of variables. Figure 33 demonstrates this behavior for spectral solutions at location 8' - 4' in the Bevatron experimental shield. It will be noted that the step-function solution shows more stable behavior than the polygonal solution.

Comparison between measured activities and activities calculated from the spectrum solution indicate that measured activities contained errors as large as 25% for threshold detectors exposed at location 8' - 4'.

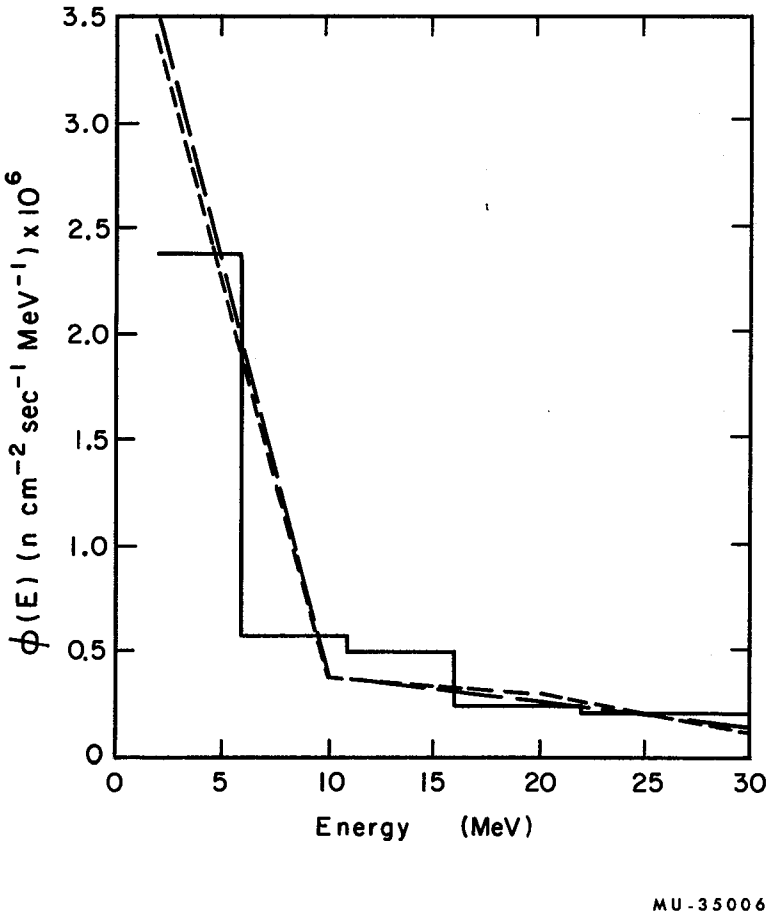

Fig. 28. Measured neutron-energy spectrum in the Bevatron shield at location 4'-1', using step function and polygonal representations. One polygonal curve (long dashes) is based on measurements of five reactions. The other polygonal curve (short dashes) is based on measurements of six reactions.

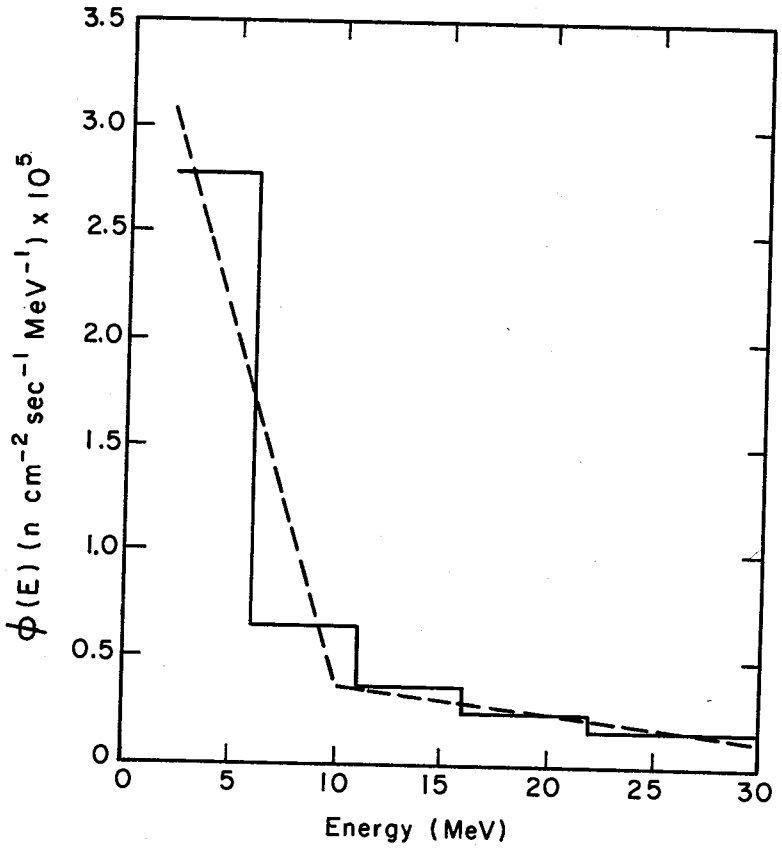

Fig. 29. Measured neutron-energy spectrum in the Bevatron shield at location 4'-3', using step-function and polygonal representations.

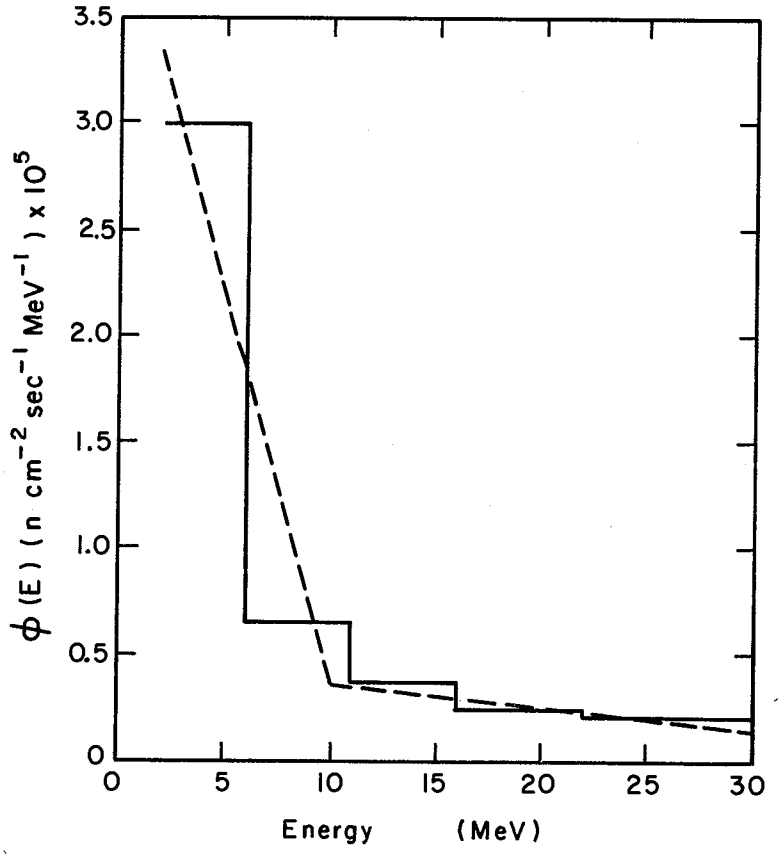

Fig. 30. Measured neutron-energy spectrum in the Bevatron shield at location 8'-2', using step-function and polygonal representations.

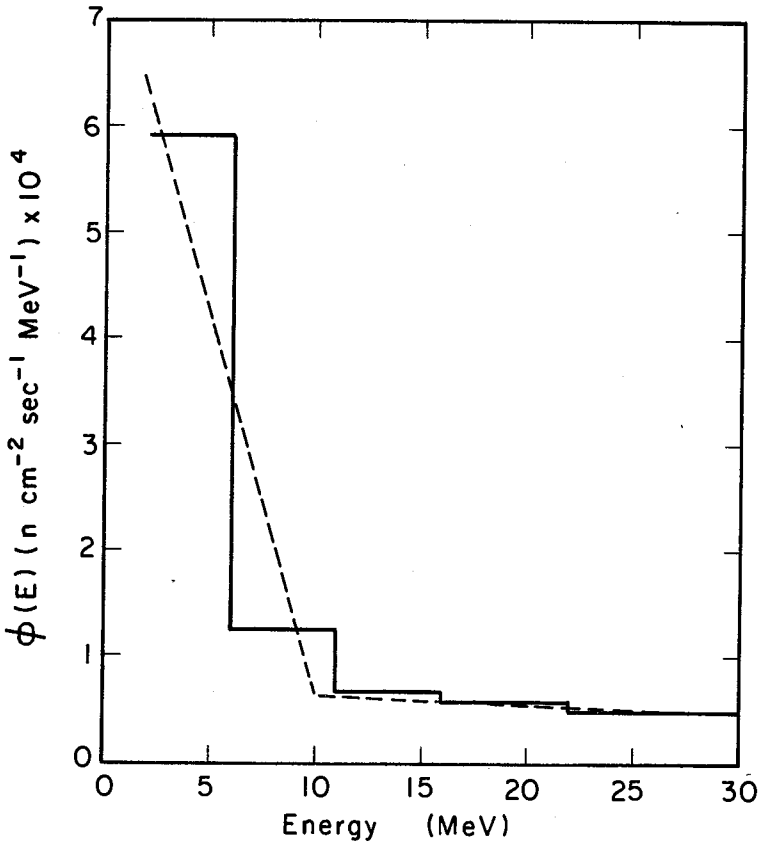

Fig. 31. Measured neutron-energy spectrum in the Bevatron shield at location 8'-4', using step-function and polygonal representations.

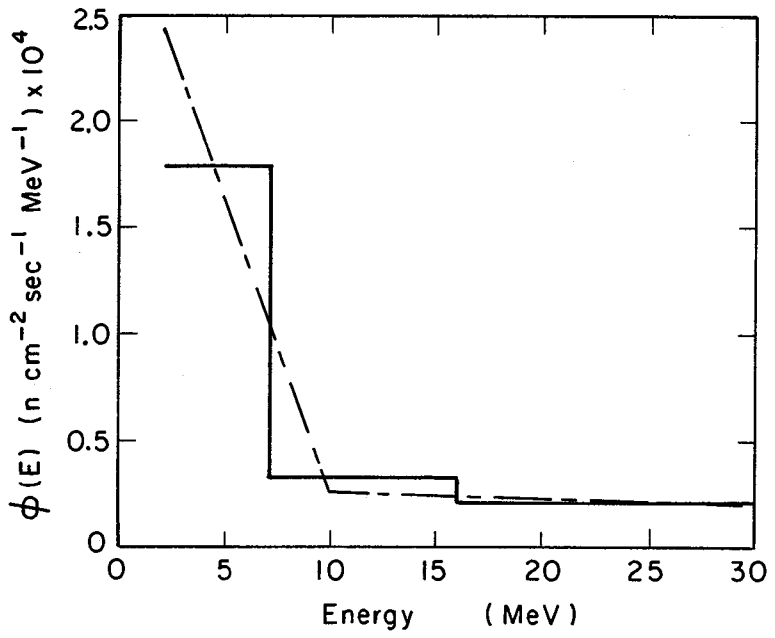

Fig. 32. Measured neutron-energy spectrum in the Bevatron shield at location 12'-3', using step-function and polygonal representations.

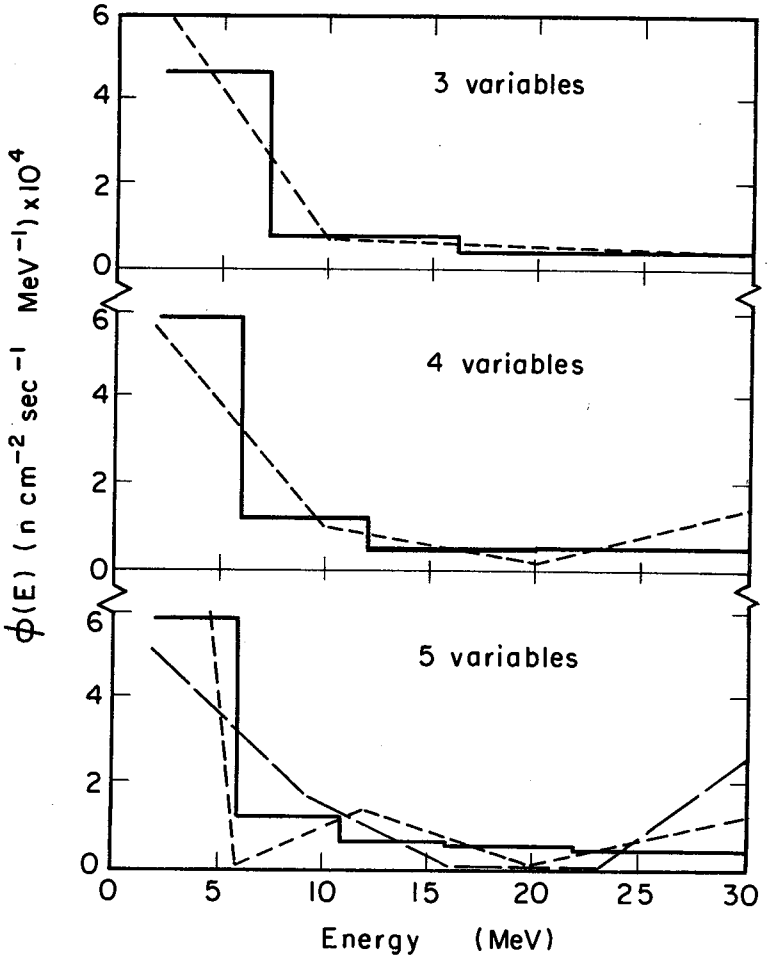

Fig. 33. Measured neutron-energy spectrum in the Bevatron shield at location 8'-4'. The same five reactions were used for all spectra. Better stability is observed for the step function. The two polygonal curves in the bottom graph show that an unstable solution has no particular pattern.

VI. SUMMARY

A method of measuring neutron spectra in the 2.5-to-30-MeV range, using threshold detectors has been improved and tested in application. Threshold reactions (n, p), (n, α), and (n, 2n) are used where the residual nucleus emits a γ ray and where neutron cross sections have been measured as a function of energy. Detectors are counted with a NaI(Tl) scintillation crystal and resulting γ spectra are analyzed by a computer program (SUPER-3). Two new computer programs (FLUXSPOS and FLUXPPOS) use least-squares analysis to solve the neutron spectrum based on input of activation and reaction-cross-section data.

The γ-spectrum-analysis method is a previous development by Dr. John Ringle[1] and is briefly described earlier in this report.

Our improved method of neutron-spectrum analysis uses experimentally determined cross sections in place of cross sections calculated by continuum-model theory. Data for cross-section measurements are taken from current literature.

In measuring the spectrum of a very-high-energy neutron source, the fraction of total activity caused by neutrons of energies below 30 MeV is estimated.

Detector activity is related to cross section and flux through Eq. (5). Once a form of the flux spectrum has been chosen (for example step function or polygon), this integral equation set may be solved by matrix-inversion techniques. However, such techniques result in oscillatory solutions where activity measurements contain substantial experimental error. A new method of solution is used in which least-squares analysis chooses flux variables such that an optimum fit is made between measured activities and activities calculated from the cross sections and flux solution. Using our technique we were able to measure spectra satisfactorily where experimental errors were unavoidably large.

The neutron spectrum of $Be^9(d, n)B^{10}$ was measured using 25-MeV deuterons and compared with other measurements of that spectrum using 24-MeV and 26-MeV deuterons. Comparison indicated that our technique was satisfactory. The spectrum was also measured for this reaction using 33-MeV deuterons.

Our technique was applied to the neutron spectra at several locations in a thick concrete shield exposed to 6.2-BeV protons. In this case the activation caused by neutrons of energies greater than 30 MeV was estimated by:

1. estimating the high-energy flux shape;
2. calculating the magnitude of that flux by measuring Be^7 activity in carbon (38.5-MeV threshold);
3. estimating high-energy-neutron cross sections on the basis of measured proton cross sections.

Although the complex γ-ray spectra in these detectors limited accuracy in determining activities, we were able to measure neutron spectra successfully with our new least-squares technique.

VII. CONCLUSIONS

Our γ-spectrum analysis method, SUPER-3 developed by Ringle[1] is quite satisfactory. It is more suitable than other methods for this application because of the accuracy with which it analyzes γ-ray spectra containing a number of unknown radioisotopes in addition to the one being analyzed. A very time consuming determination of the identity and response functions of these unknown radioisotopes would be necessary if least-squares γ-spectrum analysis were used.

New measurements of cross section for (n, p), (n, α), and (n, 2n) threshold reactions have been published and show sufficient resolution that excitation functions can be determined by drawing smooth curves through the data. Continuum-model calculations of cross sections do not dependably agree with measurements.

Two computer programs, FLUXSPOS and FLUXPPOS, successfully compute neutron spectra from activity measurements and cross sections. These programs are usable where activity data contain large experimental errors. To a great degree, these two programs avoid unstable and misleading solutions which other methods tend to give.

This improved technique is applicable to neutron spectra in the Bevatron shield, when suitable correction is made for activation by high energy particles (>30 MeV). It should be applicable to stray-neutron spectra around the Bevatron.

The resolution of this method should be improved by using more reactions than were used in spectra reported here (five to seven). It should be of interest to investigate the resolution of this method in solving for a known, artificial spectrum with known inaccuracies in activities.

ACKNOWLEDGMENTS

The author wishes to thank those individuals whose contributions have furthered this work:

Professor Roger Wallace, for suggesting this study and for his valuable supervision;

Professors Thomas H. Pigford and Richard M. Fulrath, for serving on the thesis committee;

Mr. Alan R. Smith, for his interest, patience, and frequent assistance;

Mr. William F. Dempster, Mr. Marcus W. Horowitz, and Mrs. Ardith S. Kenney, for developing and improving the computer programs;

Mrs. Nickey F. Little, for preparing data and operating computer programs.

The writer is a participant in the Naval Postgraduate Educational Program.

This work was done under the auspices of the U. S. Atomic Energy Commission.

APPENDIXES

A. Equations for Detector Activity

Our computer program, SUPER-3, determines the photopeak area, N_p, by fitting a Gaussian distribution to the corrected gamma-spectrum data (Refer to paragraph II. B. 1.) The activated threshold detector is analyzed for γ radiation and is referred to below as the source. This program computes the source disintegration rate by solving

$$A_T = \frac{N_p}{\epsilon_p \beta a (1-BT)}, \qquad (20)$$

where

- A_T = source disintegration rate in disintegrations per second,
- N_p = photopeak area in counts in peak per second,
- ϵ_p = peak efficiency in counts in peak per gamma emitted by the source,
- β = gamma branching ratio in gamma emitted by the source per disintegration,
- a = correction factor for source self-absorption, and
- BT = block time = fraction of the time the PHA does not accept pulses.

The correction factor, a, for source self-absorption may be defined further as

$$a = \frac{1-e^{-\tau t}}{\tau t}, \qquad (20)$$

where

- τ = linear γ attenuation coefficient in cm^{-1},
- t = source thickness in cm.

The source disintegration rate, A_T, may be corrected to saturation activity per target nucleus, A', by using

$$A' = \frac{A_T}{N(1-e^{-\lambda t_I}) e^{\lambda t_w}} \times \frac{\lambda t_c}{1-e^{-\lambda t_c}}, \qquad (21)$$

where

N = total number of target nuclei,
λ = decay constant for the residual nucleus in min^{-1},
t_I = irradiation time in minutes,
t_w = time between the end of irradiation and the beginning of γ counting in minutes,
t_c = time for γ counting in minutes.

If the detector is in the form of a pure element, we have

$$N = \frac{w N_0 r}{A_w} = \frac{w N_A r}{\rho},$$

where

w = detector weight in grams,
N_0 = Avogadro's number, 6.02×10^{23},
A_w = atomic weight of target element,
r = abundance of the target isotope in the target element,
N_A = atomic density in cm^{-3},
ρ = mass density in grams - cm^{-3}.

B. Reduced Experimental Data

The following table shows A_{30_i} [Eq. (5)], the detector-saturation activity caused by neutrons of less than 30-MeV energy. These saturation activities are computed from Eq. (21) and include correction for high-energy activation calculated by Eq. (18). The units are disintegrations per second per target nucleus times 10^{23}.

Reaction	Experiment						
	Deuterons on Be (d^+ energy indicated)		Bevatron shield (Location indicated)				
	25 MeV	33 MeV	4'-1'	4'-3'	8'-2'	8'-4'	12'-3'
$Ni^{58}(n, p)Co^{58}$	754,470	935,770	769,170	67,818	72,042	14,069	5,369.8
$Fe^{56}(n, p)Mn^{56}$	70,845		55,181	5,068.5	4,868.0	804.17	331.98
$Ti^{48}(n, p)Sc^{48}$	47,388	56,514					
$Mg^{24}(n, p)Na^{24}$	151,980	254,270	86,141	8,313.5	8,431.7	1,970.9	719.64
$Al^{27}(n, \alpha)Na^{24}$	88,259	140,020	55,864	4,900.3	5,234.6	1.188.6	436.14
$I^{127}(n, 2n)I^{126}$			575,150				
$Co^{59}(n, 2n)Co^{58}$	364,930	776,860	357,970	32,527	34,706	7,990.1	3,145.0
$Ni^{58}(n, 2n)Ni^{57}$	24,338	54,438					

REFERENCES

1. J. C. Ringle, A Technique for Measuring Neutron Spectra in the Range 2.5 to 30 MeV Using Threshold Detectors (Ph. D. thesis), UCRL-10732, Oct. 11, 1963.
2. H. A. Wollenberg and A. R. Smith, A Concrete Low-Background Counting Enclosure, UCRL-11454, June 15, 1964.
3. L. Salmon, Analysis of Gamma-Ray Scintillation Spectra by the Method of Least Squares, Nucl. Inst. Methods 14, 193 (1961).
4. R. L. Heath, Scintillation Spectrometry, USAEC Report IDO-16880-1, Aug. 1964, Vol. 1, Chap. IX.
5. J. Lamberieux, Activation Dosimetry and Spectrometry of Fast Neutrons, in Neutron Dosimetry, Vienna, 1963 (IAEA), Vol. II, p. 157.
6. I. Heertje and A. H. W. Aten, Jr., Determination of Cyclotron Fast Neutron Spectra and Fluxes with Activation Detectors, Physica 30, 978 (1964).
7. J. M. Blatt and V. F. Weisskopf, Theoretical Nuclear Physics, (John Wiley & Sons, Inc., New York, 1952), Chaps. VIII and IX.
8. R. G. Moore, Jr., Nuclear Reaction Cross Section Theory, Rev. Mod. Phys. 32, 101 (1960).
9. D. J. Hughes and J. A. Harvey, Neutron Cross Sections, Brookhaven National Laboratory Report BNL-325, July 1955.
10. D. J. Hughes and R. B. Schwartz, Neutron Cross Sections, Supplement No. 1, Brookhaven National Laboratory Report BNL-325, Jan. 1957.
11. R. J. Howerton, Tabulated Neutron Cross Sections, Part I, 0.001-14.5 MeV, UCRL-5226, May 1958.
12. R. J. Howerton, Semi-Empirical Neutron Cross Sections, Part II, 0.5-15 MeV, UCRL-5331, Nov. 1958.

13. R. J. Howerton (Theoretical Physics Division, Lawrence Radiation Laboratory, Livermore, California), private communication to J. C. Ringle.
14. R. Beaugé, Sections Efficaces pour les Détecteurs de Neutrons par Activation Recommandées par le Groupe de Dosimétrie d'EURATOM, NP-13722, 1963 [Service des Etudes de Protections de Piles, Centre d'Etudes Nucléaires, Fontenay-aux-Roses (Seine) France].
15. H. Liskien and A. Paulsen, Compilation of Cross-Sections for Some Neutron Induced Threshold Reactions, EUR 119.e (EURATOM, Central Bureau for Nuclear Measurements, Geel, Belgium, Aug. 1963).
16. H. Neuert and H. Pollehn, Tables of Cross Sections of Nuclear Reactions with Neutrons in the 14-15 MeV Energy Range, EUR 122.e (EURATOM, University of Hamberg, Germany, 1963).
17. J. P. Butler and D. C. Santry, Excitation Curves, Can. J. Phys. 41, 372 (1963).
18. D. C. Santry and J. P. Butler, Excitation Curves, Can. J. Phys. 42, 1029 (1964).
19. M. Bormann et al., Mesure de Quelques Sections Efficaces, J. Phys. Radium 22, 602 (1961).
20. J. M. F. Jeronymo et al., Mesure des Sections Efficaces Induites par des Neutrons, J. Phys. (Paris) 24, 816 (1963).
21. J. Picard and C. Williamson, Sections Efficaces (n, p), (n, α), et (n, 2n) sur F^{19} et Na^{23} entre 13 et 21 MeV, J. Phys. (Paris) 24, 813 (1963).
22. I. L. Preiss and R. W. Fink, New Isotopes of Cobalt; Activation Cross-Sections of Nickel, Cobalt, and Zinc for 14.8 MeV Neutrons, Nucl. Phys. 15, 326 (1960).
23. R. N. Glover and E. Weigold, Reaction Cross Sections for Cu and Ni, Nucl. Phys. 29, 309 (1962).
24. J. M. F. Jeronymo et al., Absolute Cross Sections, Nucl. Phys. 47, 157 (1963).

25. E. Saetta-Menichella et al., Statistical Model Analysis of (n, α) Reactions (I), Nucl. Phys. 51, 449 (1964).

26. U. Faechini et al., Statistical Model Analysis of (n, α) Reactions (II), Nucl. Phys. 51, 460 (1964).

27. R. J. Prestwood and B. P. Bayhurst, (n, 2n) Excitation Functions of Several Nuclei from 12.0 to 19.8 MeV, Phys. Rev. 121, 1438 (1961).

28. F. Gabbard and B. D. Kern, Cross Sections for Charged Particle Reactions Induced in Medium Weight Nuclei by Neutrons in the Energy Range 12-18 MeV, Phys. Rev. 128, 1276 (1962).

29. H. C. Martin and R. F. Taschek, The (n, γ) and (n, 2n) Reaction in Iodine, Phys. Rev. 89, 1302 (1953).

30. M. Bormann, S. Cierjacks, R. Langkau, and H. Neuert, Über die Wirkungsquerschnitte einiger n, nα-Reaktionen fur Neutronenenergien zwischen 12 und 19 MeV, Z. Physik 166, 477 (1962). A. Agodi et al., Fluctuations in Nuclear Reaction Cross-Sections, Nuovo cimento 23, 1136 (1962).

32. K. Nakai, H. Gotoh, and H. Amano, Excitation Functions of $Ni^{58}(n, p)Co^{58}$ and $Zn^{64}(n, p)Cu^{64}$ Reactions in the Energy Region from 1.8 to 4.8 MeV, J. Phys. Soc. Japan 17, 1218 (1962).

33. A. Trier, Notes on the Cross Sections for $Ti^{47}(n, p)Sc^{47}$ and $Ni^{58}(n, p)Co^{58}$, Z. Naturforschg. 17a, 275 (1962).

34. D. C. Santry (Research Chemistry Branch, Chem. & Metallurgy Div., Chalk River Nuclear Laboratories, Chalk River, Ontario), private communication, July 1964.

35. P. M. Morse and H. Feshbach, Methods of Theoretical Physics (McGraw-Hill Book Co., Inc., New York, 1953), Chap. 8.

36. W. C. Davidon, Variable Metric Method for Minimization, Argonne National Laboratory Report ANL-5990 (Rev.), Nov. 1959.

37. E. Tochilin and G. D. Kohler, Neutron Beam Characteristics from the University of California 60-in. Cyclotron, U. S. Naval Radiological Defense Laboratory Report USNRDL-TR-129, Jan. 1957.

38. A. R. Smith, J. B. McCaslin, and M. A. Pick, Radiation Field inside a Thick Concrete Shield for 6.2-BeV Incident Protons, UCRL-11331, Sept. 18, 1964.

39. N. Metropolis, R. Bivins, M. Storm, A. Turkevich, J. M. Miller, and G. Friedlander, Phys. Rev. 110, 185 and 204 (1958).

40. R. W. Wallace and B. J. Moyer, Shielding and Activation Considerations for a Meson Factory, UCRL-10086, Apr. 11, 1962.

41. J. H. Atkinson, W. N. Hess, V. Perez-Mendez, and R. Wallace, 5-BeV Neutron Cross Sections in Hydrogen and Other Elements, Phys. Rev., 123, 1850 (1961).

42. G. H. Coleman and H. A. Tewes, Nuclear Reactions of Copper with Various High-Energy Particles, Phys. Rev. 99, 288 (1955).

43. O. D. Brill, N. A. Vlasov, S. P. Kalinin, L. S. Sokolov, Cross-Section for the (n, 2n) Reaction on C^{12}, N^{14}, O^{16}, and F^{19} in the 10-37 MeV Energy Range, Doklady Akad. Nauk. 136, 55 (1961).

44. L. Marquez, Spallation of Cu with High-Energy Neutrons, Phys. Rev. 88, 225 (1952).

45. J. B. Cumming, Monitor Reactions for High Energy Proton Beams, Annual Review of Nuclear Science, (Annual Reviews, Inc., Palo Alto, California, 1963), Vol. 13, p. 261.

46. E. Bruninx, High Energy Nuclear Reaction Cross-Sections, European Organization for Nuclear Research (Geneva) Report CERN 61-1, Jan. 16, 1961.

47. E. Bruninx, High Energy Nuclear Reaction Cross-Section II, European Organization for Nuclear Research (Geneva) Report CERN 62-9, February 15, 1962.

48. E. Bruninx, High Energy Nuclear Reaction Cross-Sections III, European Organization for Nuclear Research (Geneva) Report CERN 64-17, Mar. 18, 1964.

49. J. W. Meadows and R. B. Holt, Excitation Functions for Proton Reactions with Sodium and Magnesium, Phys. Rev. 83, 47 (1951).

50. G. Rudstam, P. C. Stevenson, and R. L. Folger, Nuclear Reactions of Iron with 340-MeV Protons, Phys. Rev. 87, 358 (1952).

51. J. W. Meadows, Excitation Functions for Proton-Induced Reactions with Copper, Phys. Rev. 91, 885 (1953).

52. G. D. Wagner and E. O. Wiig, Reactions of Cobalt with Protons at 60, 100, 170, and 240 MeV, Phys. Rev. 96, 1100 (1954).

53. R. A. Sharp, R. M. Diamond, and G. Wilkinson, Nuclear Reactions of Cobalt with Protons from 0 to 100 MeV Energy, Phys. Rev. 101, 1493 (1956).

54. J. W. Meadows, R. M. Diamond, and R. A. Sharp, Excitation Functions and Yield Ratios, Phys. Rev. 102, 190 (1956).

55. S. S. Markowitz and F. S. Rowland, (p, pn) Reactions at Proton Energies from 0.3 to 3.0 BeV, Phys. Rev. 112, 1295 (1958).

56. H. P. Yule and A. Turkevich, (p, pn) Reactions in Nuclei in the 80-450 MeV Range, Phys. Rev. 118, 1591 (1960).

57. P. P. Strohal and A. A. Caretto, Jr., Excitation Functions of (p, 2 Nucleon) Reactions, Phys. Rev. 121, 1815 (1961).

58. G. V. S. Rayudu, Formation Cross Sections of Various Radio-Nuclides from Ni, Fe, Si, Mg, O, and C for Protons of Energies Between 130 and 400 MeV, Can. J. Chem., 42, 1149 (1964).

59. R. L. Lehman and O. M. Fekula, Energy Spectra of Stray Neutrons from the Bevatron, Nucleonics 11, 35 (1964).